RADC-TR-90-139
Interim Report
July 1990

TIME DOMAIN FINITE DIFFERENCE ANALYSIS OF ANTENNAS

University of California

Kenneth K. Mei

APPROVED FOR PUBLIC RELEASE; DISTRIBUTION UNLIMITED.

Rome Air Development Center
Air Force Systems Command
Griffiss Air Force Base, NY 13441-5700

This report has been reviewed by the RADC Public Affairs Division (PA) and is releasable to the National Technical Information Service (NTIS). At NTIS it will be releasable to the general public, including foreign nations.

RADC-TR-90-139 has been reviewed and is approved for publication.

APPROVED:

H. Steyskal

HANS STEYSKAL
Project Engineer

APPROVED:

John K. Schindler

JOHN K. SCHINDLER
Director of Electromagnetics

FOR THE COMMANDER: John A. Ritz

JOHN A. RITZ
Directorate of Plans and Programs

If your address has changed or if you wish to be removed from the RADC mailing list, or if the addressee is no longer employed by your organization, please notify RADC (EEAA) Hanscom AFB MA 01731-5000. This will assist us in maintaining a current mailing list.

Do not return copies of this report unless contractual obligations or notices on a specific document require that it be returned.

REPORT DOCUMENTATION PAGE

Form Approved
OPM No. 0704-0188

1. AGENCY USE ONLY (Leave Blank)	2. REPORT DATE	3. REPORT TYPE AND DATES COVERED
	July 1990	Interim Jun 88 - May 89

4. TITLE AND SUBTITLE

TIME DOMAIN FINITE DIFFERENCE ANALYSIS OF ANTENNAS

5. FUNDING NUMBERS

C - F19628-88-K-0025
PE - 61102F
PR - 2305
TA - J3
WU - 62

6. AUTHOR(S)

Kenneth K. Mei

7. PERFORMING ORGANIZATION NAME(S) AND ADDRESS(ES)

University of California
253 Cory Hall
Berkeley CA 94720

8. PERFORMING ORGANIZATION REPORT NUMBER

9. SPONSORING/MONITORING AGENCY NAME(S) AND ADDRESS(ES)

Rome Air Development Center (EEAA)
Hanscom AFB MA 01731-5000

10. SPONSORING/MONITORING AGENCY REPORT NUMBER

RADC-TR-90-139

11. SUPPLEMENTARY NOTES

RADC Project Engineer: Hans Steyskal/EEAA/(617) 377-2052

12a. DISTRIBUTION/AVAILABILITY STATEMENT

Approved for public release; distribution unlimited.

12b. DISTRIBUTION CODE

13. ABSTRACT (Maximum 200 words)

In this report, the microstrip antenna is studied as an intermediate step to the development of a broadband type flare antenna, because the microstrip antennas have been well investigated so there are plenty of results available to check our time domain technique. In fact, the microstrip antennas have many advantages of their own, such as, lightweight, low profile, low fabrication costs, and ease for mass production. Despite their obvious disadvantages of narrow bandwidth and low power capacity, the microstrip antennas have found many areas of applications.

14. SUBJECT TERMS

antennas, time domain, finite difference, analysis, patch antenna, thin substrate microstrip, thick substrate microstrip

15. NUMBER OF PAGES

56

16. PRICE CODE

17. SECURITY CLASSIFICATION OF REPORT	18. SECURITY CLASSIFICATION OF THIS PAGE	19. SECURITY CLASSIFICATION OF ABSTRACT	20. LIMITATION OF ABSTRACT
UNCLASSIFIED	UNCLASSIFIED	UNCLASSIFIED	UL

Summary

(a) ***Objective***

The purpose of this contract is to investigate the flare antennas, which are considered to be a class of broadband radiators which have minimum dispersion, so they also preserve the waveform of the input signal. Conventional broadband antennas, such as, spiral and helical antennas are very dispersive. They may be good radiators for a broadband of signals, but they do not preserve the waveform of the exciting signal. That is, a pulse input may not result in a pulse radiated.

(b) ***Technical Problems***

While the time domain method has been successfully applied to scattering and microstrip problems, their applications to antenna problems has yet to be developed. Theoretically speaking there is no difference between a scattering problem and an antenna problem. But, technically they are different. Excitation, for example, is very different between an antenna problem and a scattering. In an antenna the excitation is very localized, while in scattering it is distributed. In finite difference method, a localized excitation frequently causes stability problem. Therefore, a computer code capable of solving a scattering problem may not be able to solve an antenna problem. In this contract, our first task is to isolate the technical problems so as to make sure that the way we treat the excitation, the absorption is correct.

(c) ***Methodology***

The method to be used in this investigation is the time domain finite difference method, which has been used quite successfully in electromagnetic scattering of three dimensional objects of very complex shapes. A modified form of the method, the time domain finite element method, may be eventually partially used in this investigation, because a flare antenna involves curved edges which cannot be easily treated by the finite difference method. Additional advantages of the time domain method are the directness of the observation of the fields in time sequences and the economy of investigating the preservation of pulse shapes. Using the frequency domain method, for example, calculations of many frequencies will be required to investigate the result

of a single pulse.

(d) ***Technical Results***

The way we isolate the excitation and absorption treatment is to solve an antenna problem which is similar to the flare antenna yet has been well studied by other investigators, so that our results can be verified either theoretically or experimentally. The antenna we choose for this purpose is a patch antenna. Although a patch antenna is a narrow band antenna, its geometry has many similarities to the flare antenna. They are both composed of flat sheets and they can both be excited by microstrips and their absorption problems are similar. In an interim report (Appendix A) we are pleased to show that the results we have obtained on patch antennas are remarkably accurate compared to both theoretical and experimental results reported by other authors, indicating the integrity of the time domain method we have used.

(e) ***Important Findings and Conclusions***

In our investigation, we have found that the microstrip excitation can be modeled very accurately by the time domain method, and that the super-absorption method we have developed is a very easy-to-apply and superior technique to simulate the radiation boundary conditions. Because, by using these techniques the time domain results are well verified theoretically and experimentally based on the calculations and measurements independently done by other authors. We have concluded that the time domain method is capable of solving antenna problems including the flare antenna.

(f) ***Implications for Further Research***

Since we have confirmed the time domain finite difference method as a valid tool for antenna analysis, we are proceeding to investigate the flare antenna. Our only difficulty now is to rewrite the code for the flare antenna which involves the conforming to the curve of the flare.

(g) ***Significant Software Development***

As a by-product of this research, we have developed a software package for patch antennas. This software package is for research purpose only. It is not "friendly" enough for designing

patch antennas. A more "flexible" code is contemplated for the flare antenna.

(h) ***Special Comments***

This interim report is intended to study the excitation of co-planar sheet antennas and the new absorbing boundary condition. The patch antenna is just a convenient subject which just happen to have many available results for comparison. We do not suggest that the patch antenna is a good candidate for broadband applications; it is the flare antenna which is the objective of this research.

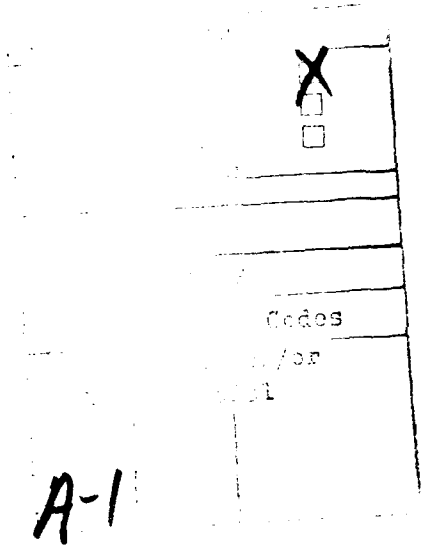

Appendix A

TIME DOMAIN FINITE DIFFERENCE ANALYSIS OF ANTENNAS—ELECTRICALLY THIN AND THICK MICROSTRIP ANTENNAS

By Kenneth K. Mei
Yong Liu
D. J. Angelakos

Electronics Research Laboratory
University of California
Berkeley, CA 94720

Sponsored by: Rome Air Development Center
Department of the Air Force
Hanscom AFB, MA 01731-5320

Contract No. F19628-88-K-0025

Table of Contents

1. INTRODUCTION

In this report the microstrip antenna is studied as an intermediate step to the development of a broadband type flare antenna, because the microstrip antennas have been well investigated so there are considerable results available to check our time domain technique. In fact, the microstrip antennas have many advantages of their own, such as, lightweight, low profile, low fabrication costs, and ease for mass production. Despite their obvious disadvantages of narrow bandwidth and low power capacity, the microstrip antennas have found many areas of applications.

The conception of microstrip antennas can be dated back to 1953 (Deschamp), however, it didn't receive wide attention until the 1970's. Presently, the properties of microstrip antennas are already very familiar to antenna engineers and the methods of analyzing microstrip antennas are also plentiful. Among the methods of analysis, the "Cavity Model" is most common (Y. T. Lo, et al. [9]). This model considers the region between the microstrip antenna and the ground plane as a cavity bounded by magnetic walls along four side edges of the antenna, and by electrical walls formed by the antenna patch and the ground plane. Therefore the fields under the patch can be assumed to be those of a cavity. The microstrip feed line is modeled by a strip current under the feeding line on one of the magnetic walls. From the cavity fields, one can obtain radiation patterns, radiated powers, resonant frequencies and input impedances at any feed point. The results are in good agreement with experiments, however, they are only good for very thin microstrip antennas and for low frequencies.

Carver and Coffey [10] used similar techniques incorporating impedance boundary conditions on the radiating walls. Good results were obtained as expected. However, there is no way to find the impedances of radiation walls analytically, so a numerical method is finally used.

Another simple and descriptive model is the Transmission Line Model [6]. In this model, the rectangular patch antenna is considered to be a line resonator without transverse field variation. The longitudinal length is about half wavelength, and the fields are radiated through the

front and end open-circuit ends via fringing effects. Simple analytical expression is obtained, which reveals the radiation mechanism, and acceptable results have been obtained.

Various numerical methods have been developed too. These include: finite element method (Carver and Coffey [10]), the wire grid model [16], integral equation method (Bailey and Deshpande [13]), moment method (Pozar [12]) etc.

All the above analyses are good only for thin substrate antennas. As the substrate becomes electrically thick, those methods either deteriorate or fail completely. In the above mentioned methods, the calculations are done in the frequency domain, which produces results of one frequency with each round of computation. Almost all of the above methods need some empirical or semi-empirical formulas or data to get a good result. The Time Domain Finite Difference (TDFD) Method we are going to use for analysis is self-consistent and avoids many shortcomings of the above methods.

The TDFD method was first introduced in 1966 by K. S. Yee [1]. This method has been widely employed by investigators in EM field. The TDFD method has many advantages. First, it discretizes Maxwell's equations into first order difference equations, yet provides second order accuracies. Secondly, there is no need to solve any matrix, the whole scheme is a simple time marching process. Thirdly, it's very suitable for analysis of planar structures because no special treatment is needed for edge fields of metals if we arrange to allow tangential **E** and vertical **H** fields to be located on metal surfaces. Finally, it has little numerical dispersion.

In this research, a pulse is sent out along the feeding microstrip line, Fig. (1). Time domain finite difference method is used to simulate the pulse propagation along the microstrip line, and the pulse reflection from, and the pulse resonance under, the microstrip patch (one can actually visualize the reflections from the end edge and side edge of the microstrip antenna). Fourier transforms are used to obtain frequency results from time domain data. Radiation patterns, resonant frequencies and input impedances of different antennas have been computed. The results are in good agreement with existing experiments or empirical formulas. It should be noted that, in

this method, (1) only one time domain simulation is needed to obtain results at all frequencies of interest. (2) In the analysis, thick substrate microstrip antennas require less memory and less computation time than thin substrate ones, because of less oscillation of fields under the patch antenna. This feature just compensates other methods in previous researchers. And (3) it can be easily used to calculate mutual couplings of microstrip antenna elements. Finally, this method is self-consistent, that is, it does not need any empirical information.

2. FORMULATION

2.1 General Descriptions

The geometry of the patch antenna is shown in Fig. (1). The related parameters are defined in Fig. (2). The feed line is embedded in the dielectric material and is electromagnetically coupled to the patch antenna. The patch is flush at the air-dielectric interface. When $mp\,1 = m\,1$, the antenna has the configuration of a conventional direct microstrip-line-fed microstrip antenna. Because of symmetry, we only need to compute half of the domain, with a magnetic wall at the center plane ($y = 0$) as a boundary.

For convenience, we assume:

1. all the conductors are perfect conductors ($a = 0$);
2. the microstrip lines and patches are infinitesimally thin;
3. the dielectric is perfect (i.e. isotropic and lossless);
4. the ground plane and the dielectric extend to infinity in y, z direction;
5. the initial fields are zero everywhere except on the front plane, where we impose some fixed boundary condition;
6. at all open side planes of the domain, on the artificial boundary, the energy storage field is negligible; and assume 1-D Sommerfeld Radiation boundary could be applied.

Assumptions 5 and 6 are concerned with the initial condition and absorbing boundary conditions for this problem, which when combined with time domain Maxwell equation give a unique solution to the fields in our computation domain.

2.2 Simulation Scheme

Yee's Lattice and Leap-Frog Scheme

Yee's lattice is shown in Fig. (3), where different electric and magnetic components occupy different space nodes. E-fields are computed only at times $t = n\ dt$ and H-fields are computed only at times $t = (n + 1/2)dt$. The leap-frog scheme reads:

$$E_x^{n+1}(i,j,k) = E_x^n(i,j,k) + \frac{dt}{\varepsilon}\left[\frac{H_z^{n+1/2}(i,j+1,k) - H_z^{n+1/2}(i,j,k)}{dy} - \frac{H_y^{n+1/2}(i,j,k+1) - H_y^{n+1/2}(i,j,k)}{dz}\right]$$

$$E_y^{n+1}(i,j,k) = E_y^n(i,j,k) + \frac{dt}{\varepsilon}\left[\frac{H_x^{n+1/2}(i,j,k+1) - H_x^{n+1/2}(i,j,k)}{dz} - \frac{H_z^{n+1/2}(i+1,j,k) - H_z^{n+1/2}(i,j,k)}{dx}\right]$$

$$E_z^{n+1}(i,j,k) = E_z^n(i,j,k) + \frac{dt}{\varepsilon}\left[\frac{H_y^{n+1/2}(i+1,j,k) - H_y^{n+1/2}(i,j,k)}{dx} - \frac{H_x^{n+1/2}(i,j+1,k) - H_x^{n+1/2}(i,j,k)}{dy}\right]$$

$$H_x^{n+1/2}(i,j,k) = H_x^{n-1/2}(i,j,k) - \frac{dt}{\mu}\left[\frac{E_z^n(i,j,k) - E_z^n(i,j-1,k)}{dy} - \frac{E_y^n(i,j,k) - E_y^n(i,j,k-1)}{dz}\right]$$

$$H_y^{n+1/2}(i,j,k) = H_y^{n-1/2}(i,j,k) - \frac{dt}{\mu}\left[\frac{E_x^n(i,j,k) - E_x^n(i,j,k-1)}{dz} - \frac{E_z^n(i,j,k) - E_z^n(i-1,j,k)}{dx}\right]$$

$$H_z^{n+1/2}(i,j,k) = H_z^{n-1/2}(i,j,k) - \frac{dt}{\mu}\left[\frac{E_y^n(i,j,k) - E_y^n(i-1,j,k)}{dx} - \frac{E_x^n(i,j,k) - E_x^n(i,j-1,k)}{dz}\right] \quad (1)$$

It is obvious in the first 3 equations of (1) that if the $(n+1/2)dt$ is the present time, then the E fields of the future time $(n+1)dt$ can be calculated from the present H and past E fields. The last 3 equations of (1) calculates the future H fields from the present E fields and past H fields.

For details, please refer to [2], [4].

By updating the fields according to these formulas, we can simulate pulse propagation, reflection from the patch and resonance under the patch. The absorbing boundary conditions simulate the radiation of fields, and the leakage of surface waves.

2.3 Radiation Pattern

To find the radiation fields in the space above the substrate, we apply the principle of equivalent sources. There are many ways to do so. Since the TDFD method provides fields every-

where in the computational domain at all time of the simulation, we can actually choose any closed surface for the equivalent sources. Of course, we need to choose one which is most convenient for integration to find the far fields. And, for that reason, we choose the air-substrate interface as the surface on which the equivalent sources are located. In our calculation, we choose the magnetic current on perfectly conducting surface as the basis for equivalent sources. The magnetic currents are the tangential electric fields on the air substrate interface. Since the sources are backed by electrically conducting plane, the radiated fields are equivalent to radiation from $\mathbf{J}_m$ in free space, where

$$\mathbf{J}_m = 2\,\mathbf{E} \times \hat{n} \tag{2}$$

Where $\hat{n}$ is the unit vector perpendicular to the surface of equivalent current. The bold face variables represent vectors. The schematics of the equivalent sources are shown in Fig. (4).

We may also use equivalent electric current on magnetic walls for the same computation. There does not seem to be any difference in the choices.

It is obvious that the time domain data of the magnetic current is too large to store in computer memory. So, as the computation marches on, Fourier Transform of the magnetic current is calculated simultaneously,

$$\mathbf{J}_m(\omega) = \int_0^\infty \mathbf{J}_m(t) e^{-j\omega t}\, dt \tag{3}$$

The magnetic current is then extended to the left half plane by image of the magnetic wall of Fig. (2). Where,

$$J_{my}(-y, z, \omega) = J_{my}(y, z, \omega)$$

$$J_{mz}(-y, z, \omega) = -J_{mz}(y, z, \omega)$$

Here for convenience, we change the coordinates (Fig. (5), (6)).

$$J_{mz}(y, z, \omega) \rightarrow J_{my}(x, y, \omega)$$

$$J_{my}(y, z, \omega) \rightarrow J_{mx}(x, y, \omega)$$

The far field potentials due to the magnetic current are given by:

$$F_x(r,\omega) = \frac{\varepsilon_0}{4\pi}\frac{e^{-jk_0 r}}{r}\int_0^b \int_{-\frac{a}{2}}^{\frac{a}{2}} J_{mx}(x,y,\omega) e^{jk_0(x\sin\theta\cos\psi+(y-\frac{b}{2})\sin\theta\sin\psi)}dx\,dy \tag{4a}$$

$$F_y(r,\omega) = \frac{\varepsilon_0}{4\pi}\frac{e^{-jk_0 r}}{r}\int_0^b \int_{-\frac{a}{2}}^{\frac{a}{2}} J_{my}(x,y,\omega) e^{jk_0(x\sin\theta\cos\psi+(y-\frac{b}{2})\sin\theta\sin\psi)}dx\,dy \tag{4b}$$

The far fields are given by

$$H_\theta(\theta,\psi,\omega) = -j\,\omega F_x(\theta,\psi,\omega)\cos\theta\cos\psi - j\,\omega F_y(\theta,\psi,\omega)\cos\theta\sin\psi \tag{5a}$$

$$H_\psi(\theta,\psi,\omega) = j\,\omega F_x(\theta,\psi,\omega)\sin\psi - j\,\omega F_y(\theta,\psi,\omega)\cos\psi \tag{5b}$$

$$E_\psi = -Z_0 H_\theta \tag{5c}$$

$$E_\theta = Z_0 H_\psi \tag{5d}$$

where $Z_0 = 376\ \Omega$ is the free-space impedance. To get the radiation pattern, we can take off the factor $\frac{e^{-jk_0 r}}{r}$ in the computation of F_x and F_y. That is,

$$D(\theta,\psi,\omega) \propto (|H_\theta|^2 + |H_\psi|^2) \tag{6}$$

Radiated power can be found through

$$P_r(\omega) = \frac{1}{2} Z_0 \iint_{4\pi} (|H_\theta|^2 + |H_\psi|^2) r^2\, d\Omega \tag{7}$$

2.4 Current, Voltage and Propagation Constant

As we all know, a microstrip lines does not support TEM modes. However, it supports quasi-TEM modes. Hence we can define currents and voltages with good enough unambiguity. At any reference plane z=constant, the voltage and current are given by

$$V(z,\omega) = \frac{2}{w}\int_0^{\frac{g}{2}} \int_0^h E_x(x,y,z,\omega)dx\,dy \tag{8}$$

$$I(z,\omega) = 2\int_l \mathbf{H}_y(z,\omega)\cdot \mathbf{dl} \tag{9}$$

Where l is the path surrounding half the metal strip. The integration along y direction in the voltage expression is used to average the voltage along y when w/h is small. It's obvious that we want to calculate these quantity at points far from the feeding point to avoid higher order modes.

The propagation constant $\gamma(\omega) = \alpha + j\beta$ is found from calculation of uniform microstrip transmission line by

$$e^{-\gamma(\omega)(z_j - z_i)} = \frac{V(z_j, \omega)}{V(z_i, \omega)} \tag{10}$$

2.5 Input Impedances and Resonant Frequencies

The complex power delivered through an antenna loaded microstrip line (P_t) includes power radiated through the microstrip antenna (P_r), the power leaked through surface wave (P_s) which is supported by the dielectric substrate, and the power consumed by the artificial absorbing boundary condition and damping absorbing boundary condition at the side plane (P_b).

$$P_t = P_r + P_s + P_b \tag{11}$$

When the computation domain is not large enough, or the artificial absorbing is too close to the near field, P_b become significant and the accuracy of impedances becomes questionable.

The formula that give the power transfer at any reference plane z=contant. are

$$P_t(z, \omega) = 2 \iint_S (E_x H_y^* - E_y H_x^*)\, dx\, dy = \frac{1}{2} V I^* = \frac{1}{2} Y_{in} |V|^2 = \frac{1}{2} Z_{in} |I|^2 \tag{12}$$

Where S is the area of half cross section of the computation domain. Hence the input impedance has 3 definitions

1) $$Z_{in}(z, \omega) = \frac{V(z, \omega)}{I(z, \omega)} \tag{13a}$$

2) $$Z_{in}(z, \omega) = \frac{2P(z, \omega)}{|I(z, \omega)|^2} \tag{13b}$$

3) $$Z_{in}(z, \omega) = \frac{|V(z, \omega)|^2}{2P(z, \omega)} \tag{13c}$$

Calculations have shown that all the above definitions end up with almost the same Z_{in}. This confirms that the previous definition of current and voltage are meaningful.

When the configuration is just a transmission line, the input impedance become characteristic impedance ($Z_c = Z_{in}$).

To obtain the input impedance at feeding point, we calculate the input impedance at a z first, then transfer it to the feeding point $z = z_0$, to avoid near fields.

$$Z_{in}(z,\omega) = \frac{V(z,\omega)}{I(z,\omega)} \tag{14a}$$

$$\Gamma(z,\omega) = \frac{Z_{in}(z,\omega) - Z_c(\omega)}{Z_{in}(z,\omega) + Z_c(\omega)} \tag{14b}$$

$$\Gamma(z_0,\omega) = \Gamma(z,\omega)e^{2\gamma(z-z_0)} \tag{14c}$$

$$Z_{in}(z_0,\omega) = Z_c(\omega)\,\frac{1+\Gamma(z_0,\omega)}{1-\Gamma(z_0,\omega)} \tag{14d}$$

The resonant frequency is defined as the frequency when the imaginary component of input impedance is zero. If we write

$$Z_{in}(z_0,\omega_0) = R(z_0,\omega_0) + j\,X(z_0,\omega_0)$$

then at resonance

$$X(z_0,\omega_0) = 0$$

and $R(z_0,\omega_0)$ is the resonant resistance.

3. NUMERICAL TECHNIQUE AND CONSIDERATIONS

3.1 Excitation Pulse

The pulse is excited by setting E_x under the microstrip to be the prescribed waveform varying with time steps, and E_x elsewhere on front plane to be zero. Other tangential field component on the front plane are set to zero all the time. This kind of arrangement need some time for the wave to travel some distance to change to the real distribution. This scheme also generate some DC magnetic field near the front plane. This DC field, though not harmful to the traveling wave, can cause trouble when you change the boundary condition at the front plane.

3.2 Boundary Conditions

Although we are dealing with an open structure we still need to confine our computational domain to a closed surface boundary. On that surface, we use absorbing boundary condition to simulate wave propagation in free space, i.e. to make the boundary transparent to EM waves. Generally, it is impractical to simulate the perfect absorbing boundary condition because it requires knowledge of electrical and magnetic tangential fields on the closed surface for all past

time. Since the field on the boundary is mainly determined by the most recent fields of nearby space region, many schemes have been constructed utilizing local field to approximate perfect radiation boundary condition. Here we have chosen simple shift plus super-absorbing boundary condition for its simplicity of implementation and high accuracy. Damping absorbing boundary condition is also chosen to stabilize the whole leap-frog scheme.

(a) ***Super-absorption***

The super-absorbing boundary condition is not in itself a boundary condition, but a scheme that can be applied to other existing boundary condition and get better result than the original one does. Mei has found that, if one applies an absorbing boundary condition on **H** to get $\mathbf{H}_1$, at a boundary wall and applies the same boundary condition on **E** to get $\mathbf{E}_2$, and compute $\mathbf{H}_2$ at the same point as $\mathbf{H}_1$ through leap-frog scheme from $\mathbf{E}_2$, then the error due to imperfect absorbing boundary condition in $\mathbf{H}_1$ and $\mathbf{H}_2$ possess opposite sight. Hence, by proper linear combination of $\mathbf{H}_1$ and $\mathbf{H}_2$, we can cancel the errors due to reflection.

(b) ***Damping***

The basic idea of damping absorbing condition is to simply assign some buffer layer right inside the boundary, which has proper electrical and magnetic loss and become larger and larger toward the outer boundary. The EM energy can be dissipated in this damping layer with little reflection. The loss terms enter Maxwell equation as follows,

$$\frac{\partial \mathbf{E}}{\partial t} = \frac{1}{\varepsilon} \nabla \times \mathbf{H} - \gamma \mathbf{E} \tag{15a}$$

$$\frac{\partial \mathbf{H}}{\partial t} = \frac{1}{\mu} \nabla \times \mathbf{E} - \gamma \mathbf{H} \tag{15b}$$

It's easy to show that the wave impedance $Z_0 = \sqrt{\frac{\mu_c}{\varepsilon_c}} = \sqrt{\frac{\mu}{\varepsilon}}$. Hence there would be no reflection for normal incident plane waves. The TDFD leap-frog scheme for equation (15) can be approximated as follows

$$\mathbf{E}^{n+1} = (1 - \Delta t\ \gamma)\, \mathbf{E}_I^{n+1} \tag{16a}$$

$$\mathbf{H}^{n+1/2} = (1 - \Delta t\ \gamma)\,\mathbf{H}_f^{n+1/2} \tag{16b}$$

where $\mathbf{E}_f^{n+1}$, $\mathbf{H}_f^{n+1/2}$ are obtained by the original scheme when $\gamma = 0$. Define $d(\mathbf{r}) = [1 - \Delta t\ \gamma(\mathbf{r})]$, then the damping boundary condition is simply implemented by multiplying the field obtained from normal scheme (1) by $d(\mathbf{r})$. A different function form of $d(\mathbf{r})$ results in different percentage of reflection. In this program, we have chosen $d(z)$ to be in the form of $e^{-\alpha z^2}$.

In this calculation, we have chosen the computation domain to be a box [2]. And the surfaces of the box are parallel to the coordinate surfaces. On the center plane, we apply boundary condition of a magnetic wall, i.e., tangential magnetic fields are anti-symmetrical, tangential electrical fields are symmetrical. The bottom plane is a electrical conductor of the substrate. On the other end plane, we use a simple shift of previous fields at some inner layer as the new fields on end plane to simulate the propagation of waves. On the side and upper planes, since there is no outgoing wave, the fields should die off compared to the inner layers, but the field should have the same phase as their inner layers. For simplicity, we obtain the boundary fields by shifting the fields one space step from the inner layer of one earlier time step. This arrangement can introduce some loss of EM energy because the boundary condition is really a radiation boundary condition. If we don't move the side boundary far enough from the patch antenna, energy loss will become serious, which greatly influences the calculated input impedance lever of antenna. As for the front plane, which contains the excitation some special treatment is needed. We need to excite the input pulse here, and yet wish this plane to be transparent to the reflected pulses. To accomplish this, we first apply a fixed boundary conditions to generate the pulse and after the pulse have passed we switch to an absorbing boundary condition there. Here, we have applied both the damping absorbing boundary condition [17] and the super-absorbing boundary condition to get a good absorption as well as stability for the leap-frog scheme.

3.3 Stability

According to [5], an initial boundary value problem is stable if and only if

(1) the Courant stability condition given by equation (17) is satisfied everywhere inside the finite element mesh region,

$$v_{max}\, dt \le \frac{1}{\sqrt{\frac{1}{dx^2} + \frac{1}{dy^2} + \frac{1}{dz^2}}} \tag{17}$$

(2) the numerical model (including boundary conditions) admits no plane wave solutions that grow from each time step to the next by a constant factor absolutely greater than one, and

(3) the model (including boundary conditions) admits no wave solutions with group velocities which support active radiation of computation.

One can always choose dt, dx, dy, dz to satisfy condition (1) if computer capacity allows. However, it is usually too complicated for us to be able to check conditions (2) and (3).

Since it is impossible to eliminate reflection completely by the absorbing boundary conditions and conditions (2) & (3) are uncertain, we have no guarantee that the computation will be stable. Instabilities caused by reflections from absorbing walls were reported by Zhang [4]. Zhang was able to avoid instability of the microstrip problem by truncating the time domain data before major reflections from boundaries return. Unfortunately, the truncation trick cannot be applied to the antenna problem, because a microstrip antenna, especially those with thin substrates, must go through several oscillations before the fields within the patch are diminished to negligible amount.

Another stability problem is related to the switching of boundary conditions at the front plane, i.e., the plane of excitation. As we have mentioned earlier, the plane containing the excitation is a short circuit except at the microstrip. This short circuit plane is switched to be an absorbing plane after the excitation pulse has passed. This switching of boundary conditions actually causes instability.

The damping method of absorption adds stability to the time domain method, because it always dissipate energy in the solution process. But, the damping method is very demanding on memory. Usually it takes about 60 extra space steps on each side of the boundary wall to reduce the reflection down to acceptable level.

In this investigation, we have combined the damping technique with the super-absorption method, and have found that only an extra 20 space steps at the excitation wall and the end wall (the wall opposite to the excitation plane) is sufficient to reduce reflections and stabilize the solution.

3.4 Choice of Parameters

The excitation is chosen to be a Gaussian pulse since the Gaussian pulse and it's Fourier Transform (also a Gaussian) have a smooth waveform yet can give enough frequency range. The pulse is in the form

$$E_x(t) = \exp\left[-\frac{(t-t_0)^2}{T^2}\right] \tag{18}$$

Where t_0 is chosen to be large enough to suppress the discontinuity introduced by turning on the signal at t=0. T is chosen to adjust the pulse width to be wide enough so that its discrete representation in space is well behaved and yet kept narrow to save computation time. Typical values chosen are

$$t_0 = 140\,dt$$

$$T = 40\,dt$$

The parameters which describe the structure discretization computed are defined in Fig. (2). The discretization of the computational domain are not the same in the x,y,z directions. Let $dx = 1$, and $dy = r_2$ and $dz = r_3$. We have to choose r_2 small to allow discrete representation of the microstrip but not too small to exhaust the computer memory. r_3 is chosen so that the Courant condition of (17) is satisfied in free space and also in the substrate. Since the wave travels slower in the substrate, the ratio $k = \frac{vdt}{dz}$ is chosen to be 1/6 to 1/7.

4. NUMERICAL RESULTS

In the following, we have computed different cases for both thin and thick microstrip antenna. Results are compared with those of other authors or with empirical formulas. Reasonably good agreement is shown. Only the lowest resonant frequency is considered here. All the

patch antennas are fed at center of the width by microstrip lines.

4.1 General Description—Qualitative

Plot in Fig. (7)–Fig. (10) are E_x fields just underneath the microstrip line and patch antenna. Figure (7) shows the Gaussian pulse traveling down the microstrip line. Figure (8) shows the same pulse shortly after it hit the front edge of the patch. Figure (9) shows part of the pulse reflected back by the front edge of the patch antenna, part of it continue traveling down along the patch antenna. Figure (10) is at the state of resonance. The pulse bounce back and forth between the front edge and end edge of the patch antenna.

Figures (11) and (12) show how the current and voltage pulses are reflected back from edges of the patch antenna. These waveforms are for different locations along the microstrip feed line. The 1st peak in the waveform is the input pulse, the 2nd one is the reflection from front edge of the patch antenna, the 3rd one, the small peak, is the reflection from side edge of the patch, the 4th peak is from the end edge of the patch and so on. As we can see, the reflected wave decays very slowly for electrically thin microstrip antenna.

Figures (13)–(14) show the amplitude distribution of the equivalent magnetic current at resonant frequency. Figure (13) is for J_{mz}, Fig. (14) is for J_{my}. Clearly seen in the figure is that the field have no variation along the width of the antenna. The variation along the length of the antenna is sinusoidal like. This implies that the cavity model and transmission line model are reasonable. We should also notice that TDFD method have taken into account the effect of the microstrip feed line, because the magnetic current there is exactly zero. Notice the difference of fields between the front edge and end edge of the antenna due to traveling wave effect. This deviation of calculated fields from cavity mode fields does not have much effect on the symmetry of radiation pattern near the resonant frequency, but does have an effect of resonance.

Figures (15) and (16) show the radiation patterns at resonant frequency. Shown on Fig. (15) is the E_θ component on E-plane, where E_ψ component is negligible. Figure (16) shows the E_ψ component on H-plane where the component E_θ is negligible. The coordinate which correspond

to the definition of θ and ψ is shown in Figs. (5), (6). The radiation pattern do not change much near resonant frequency, and radiation pattern for different patch antennas are about the same at the first resonant frequency. A general case when it's off resonant frequency is shown in Fig. (17)–(18), where we can see the unsymmetrical radiation pattern. This unsymmetry comes from the feeding system which is unsymmetrical, and because the fields distribution under the microstrip antenna are really unsymmetrical in general.

4.2 Comparison Results—Quantitative

4.2.1 *Electrically Thin Substrate Microstrip Antenna*

Case 1

Parameters used in the following computation are:

PARAMETERS	VALUES	DISCRETIZATION
Substrate thickness	$h = 0.159$ cm	$mp1 = m1 = 4$
Width of the feeding microstrip line	$w = 0.447$ cm	$m2 = 3$
Width of microstrip antenna	$a = 4.02$ cm	$2\,mp2 = 54$
Length of microstrip antenna	$b = 4.02$ cm	$mp32 - mp31 = 54$
Substrate dielectric constant	$\varepsilon_r = 2.55$	
Space scaling factor	$r_1 = 1.0$	
	$r_1 = 1.0$	
	$r_2 = 1.8742133$	
	$r_3 = 1.8742133$	
The constant k	$k = 0.389165393$	

The Computation Domain: $(n1 \times n2 \times n3) = (30 \times 50 \times 170)$

Time steps taken: $nt = 7300$.

CPU time needed on Cray-1: 1102 seconds

Figure (19) is the Smith Chart which gives the input impedance loci near resonant frequency compared to experiment results obtained by Pozar [12]. The resonant frequency is the frequency where the impedance loci crosses the real axis of the Smith Chart. The key parameters at resonant frequency are:

Items	f_0	$R(f_0)$
Experiment	2.270	411 Ω
TDFD	2.220	427 Ω

The slight difference in resonant frequency and the resonant input impedances between our theoretical results and Pozar's experimental may just be the difference in feeding arrangement between our model (using microstrip) and his experiment (using coaxial line). In any case, the agreement is quite remarkable.

Case 2

In the following, resonant frequency obtained by TDFD method is compared with Y. T. Lo's results. Good agreements are observed. Parameters for this computation are

$$a = 7.6 \text{ cm}$$
$$b = 11.4 \text{ cm}$$
$$w = 0.437 \text{ cm}$$
$$h = 0.159 \text{ cm}$$
$$\varepsilon_r = 2.62$$

The resonant frequencies obtained are:

Lo's experiment	Lo's theory	TDFD method
0.803 GHz	0.813 GHz	0.797 GHz

4.2.2 *Electrically Thick Substrate Microstrip Antenna*

As indicated before, the TDFD method can handle electrically thick substrate antenna better than thin ones. In the following examples, the memory requirement for a thick substrate antenna is somewhat relaxed and the time steps needed is about only one third of that needed for thin substrate antennas. The problem of instability due to changing of boundary condition on the front plane is less significant here. The reason for needing less time steps is that the electrically thick substrate microstrip antennas are more efficient radiators, so there are less oscillations within the

antenna.

In all the following computations, the substrate thickness is 0.3175 cm, the relative dielectric constant of the substrate is 2.33.

Figures (20)–(24) shows input impedance loci for different antenna patch size. The input impedances are normalized to 50 Ω.

Not much work on electrically thick substrate microstrip antenna has been done. Chang [14] has done some measurements on resonant frequency of thick substrate antennas. He used a coaxial line as the feed. And because of noises in the measurement, there was no zero reactance of input impedance, hence he defined resonant frequency to be the frequency when real part of input impedance is maximum. From our experience in the calculations, resonant frequency is sensitive to feed arrangement. Therefore it is not proper to compare our results to Chang's results. We compare instead to the results obtained by an empirical formula.

From the impedance locis, we obtain resonant frequencies. These results are compared to the empirical formula ([18] pp. 46, 57). Good agreement (within 4%) can be seen. It should be noticed that the empirical formula was not meant to predict resonant frequencies for electrically thick substrate antennas. The formulas used are given as follows

The effective dielectric constant is

$$\varepsilon_{eff}(w) = \frac{\varepsilon_r + 1}{2} + \frac{\varepsilon_r - 1}{2}\left[1 + 12\frac{h}{w}\right]^{-\frac{1}{2}}$$

Where w is the width of the patch antenna in our calculation.

The effective extension of patch length is

$$\Delta b = \frac{0.412(\varepsilon_{eff}(a) + 0.3)\left[\frac{a}{h} + 0.264\right]}{(\varepsilon_{eff}(a) - 0.258)\left[\frac{a}{h} + 0.8\right]}$$

The predicted resonant frequency is

$$f_r = \frac{c}{2(b + 2\Delta b)\sqrt{\varepsilon_{eff}}}$$

Where c is the speed of the light. b is the length of the antenna.

Comparison of resonant frequencies for different antenna sizes are shown in the following table

a	b	f_r (empirical)	f_r (TDFD)
1.7	1.1	7.4	7.56
1.4	0.9	8.71	8.93
1.2	0.8	9.57	9.9
1.05	0.7	10.6	10.95
0.9	0.6	11.9	12.33

5. CONCLUSION

The time domain finite difference method has been successfully applied to a class of microstrip antennas. It has been shown with convincing evidences that the modeling of the feed and the advanced absorbing boundary conditions we have used are good dependable techniques to make the TDFD method practical. It has also been shown that the method is more efficient for broadband antennas than for narrow band antennas. We are confident that this technique will enable us to solve the flare antenna even with greater confidence. Using the patch antenna as a vehicle we have isolated the feeding and absorption problems and convinced ourself that those problems have been solved. We can now proceed to our final objective of solving the pulse radiating antennas.

REFERENCE

1. K. S. Yee, "Numerical Solution of Initial Boundary Value Problems Involving Maxwell's Equations in Isotropic Media," *IEEE Trans. on Antennas and Propagation*, Vol. AP-14, pp. 302–307, May 1966.

2. A. Taflove, M. E. Brodwin, "Numerical Solution of Steady-State Electromagnetic Scattering Problems Using the Time-Dependent Maxwell's Equations," *IEEE Trans. on Microwave Theory and Techniques*, Vol. MTT-23, pp. 623–630, 1975.

3. K. K. Mei, A. C. Cangellaris, and D. J. Angelakos, "Conformal Time Domain Finite Difference Method," *Radio Science*, Vol. 19, pp. 1145–1147, Sept.–Oct. 1984.

4. X. Zhang, J. Fang, K. K. Mei, and Y. Liu, "Calculation of the Dispersive Characteristics of Microstrips by the Time-Domain Finite Difference Method," *IEEE Trans. on Microwave Theory and Techniques*, Vol. MTT-36, pp. 263, 267, February 1988.

5. C. C. Lin, "Numerical Model of Two-Dimensional Time Domain Electromagnetic Scattering by Underground Inhomogeneities," Ph.D Dissertation, Dept. EECS, University of California, Berkeley, 1985.

6. R. E. Munson, "Conformal Microstrip Antennas and Microstrip Phased Arrays," *IEEE Trans. on Antennas and Propagation*, Vol. AP-22, pp. 74–78, 1974.

7. A. G. Derneryd, "Microstrip Array Antenna," Proc. 6th European Microwave Conference, pp. 339–343, 1976.

8. P. K. Agrawal and M. C. Bailey, "An Analysis Technique for Microstrip Antennas," *IEEE AP-S Int. Symp. Digest*, pp. 395–398, 1976.

9. Y. T. Lo, D. Solomon, and W. F. Richards, "Theory and Experiment on Microstrip Antennas," *IEEE Trans. on Antennas and Propagation*, Vol. AP-27, pp. 137–145. 1979.

10. K. R. Carver and E. L. Coffey, "Theoretical Investigation of the Microstrip Antenna," Tech. Rept. PT-00929, Physical Science Laboratory New Mexico State University, Las Cruces (New Mexico), January 1979.

11. M. D. Deshpande and M. C. Bailey, "Input Impedance of Microstrip Antennas," *IEEE Trans. on Antennas and Propagation*, Vol. AP-30, pp. 645–650, July 1982.

12. D. M. Pozar, "Input Impedance and Mutual Coupling of Rectangular Microstrip Antennas," *IEEE Trans. on Antennas and Propagation*, Vol. AP-30, pp. 1191–1196, November 1982.

13. M. C. Bailey and M. C. Deshpande, "Integral Equation Formulation of Microstrip Antennas," *IEEE Trans. on Antennas and Propagation*, Vol. AP-30, pp. 651–656, July 1982.

14. E. Chang, S. A. Long, and W. F. Richards, "An Experimental Investigation of Electrically Thick Rectangular Microstrip Antennas," *IEEE Trans. on Antennas and Propagation*, Vol. AP-34, pp. 767–772, June 1986.

15. J. Y. Fang, "On Radiation Boundary Conditions for One Dimensional Wave Equation," MS Thesis, University of California, Berkeley, May 1987.

16. P. K. Agrawal and M. C. Bailey, "An Analysis Technique for Microstrip Antennas," *IEEE Trans. on Antennas and Propagation*, Vol. AP-25, pp. 756–759, 1977.

17. J. Y. Fang and S. K. Chang, "Evaluation of Elastic Wave Absorbing Boundary Conditions by Damping," to be published.

18. I. J. Bahl and P. Bharia, "Microstrip Antennas," Artech House, Inc., 1980.

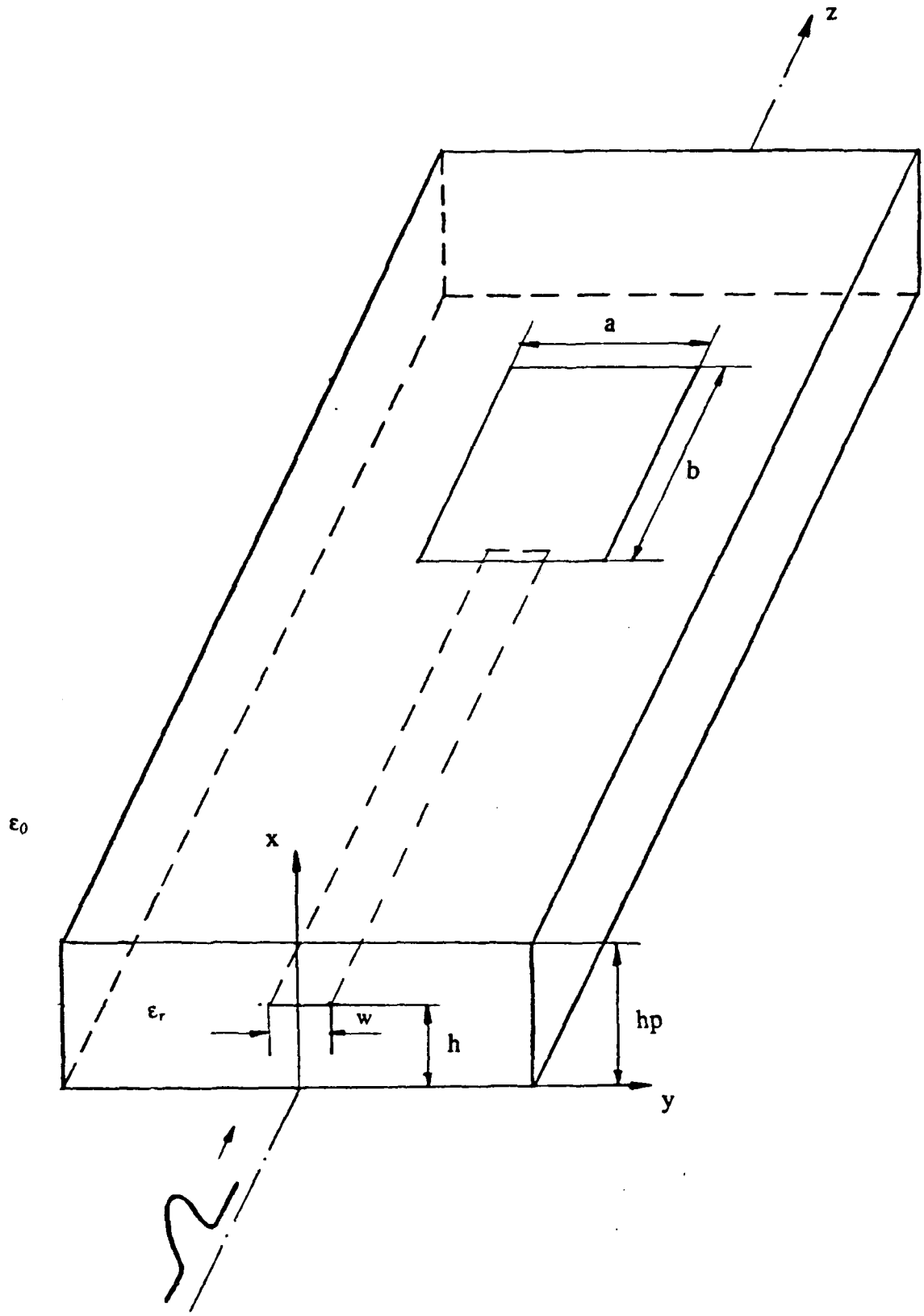

Fig. (1) A rectangular microstrip antenna fed by microstrip line.

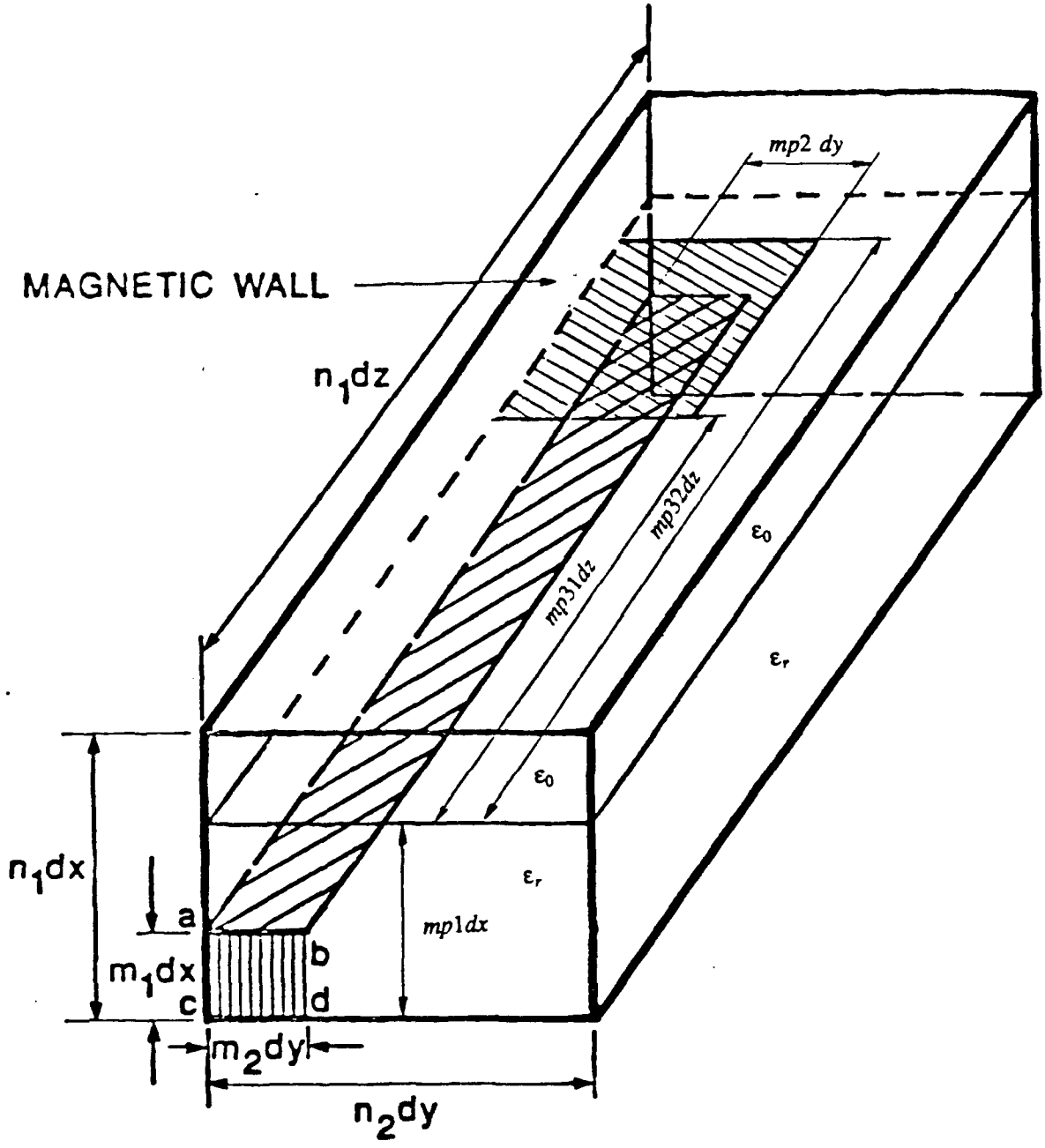

Fig. (2) Computation domain and definitions of quantized parameters.

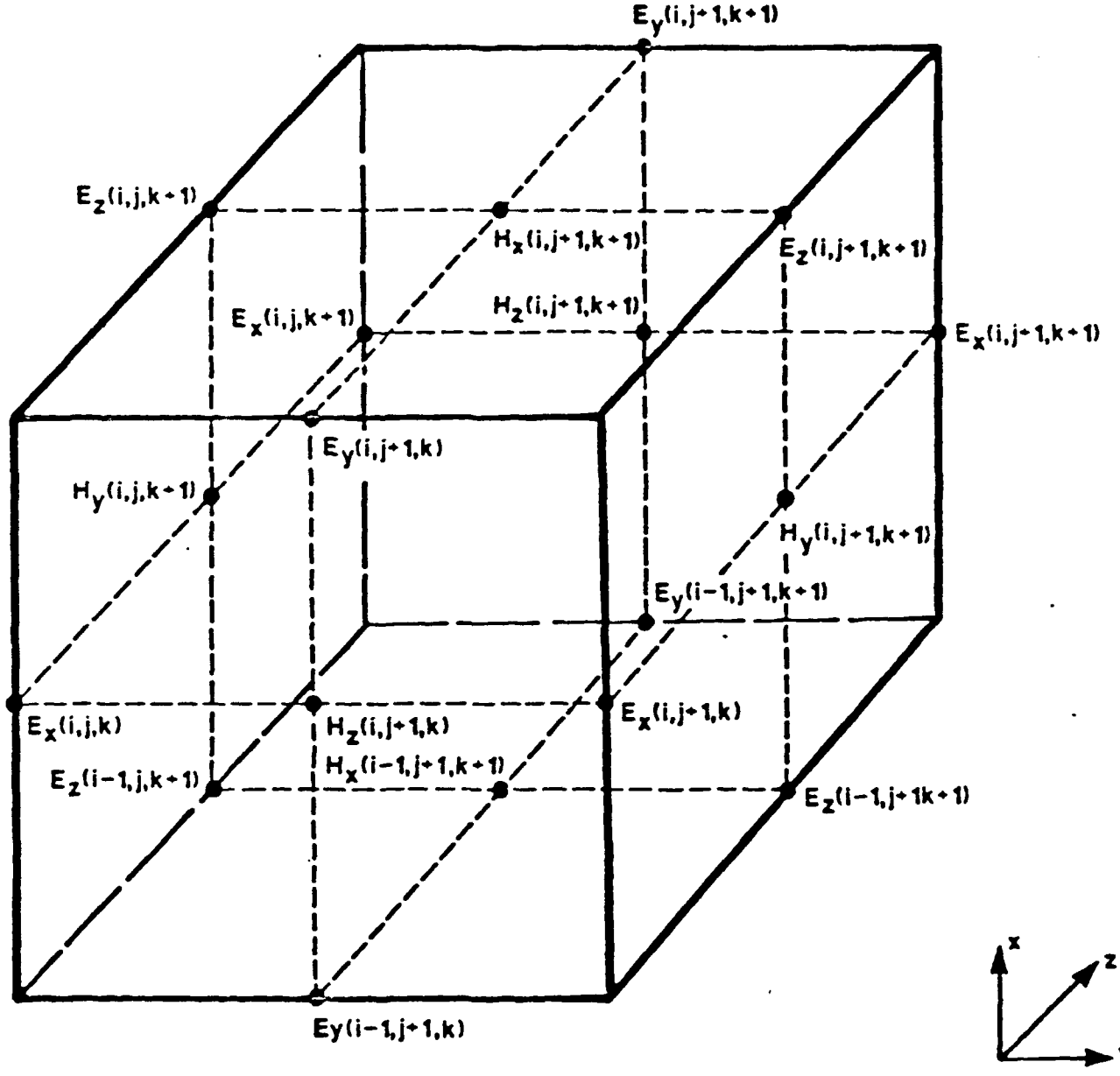

Fig. (3) Yee's nodal distributions of field components.

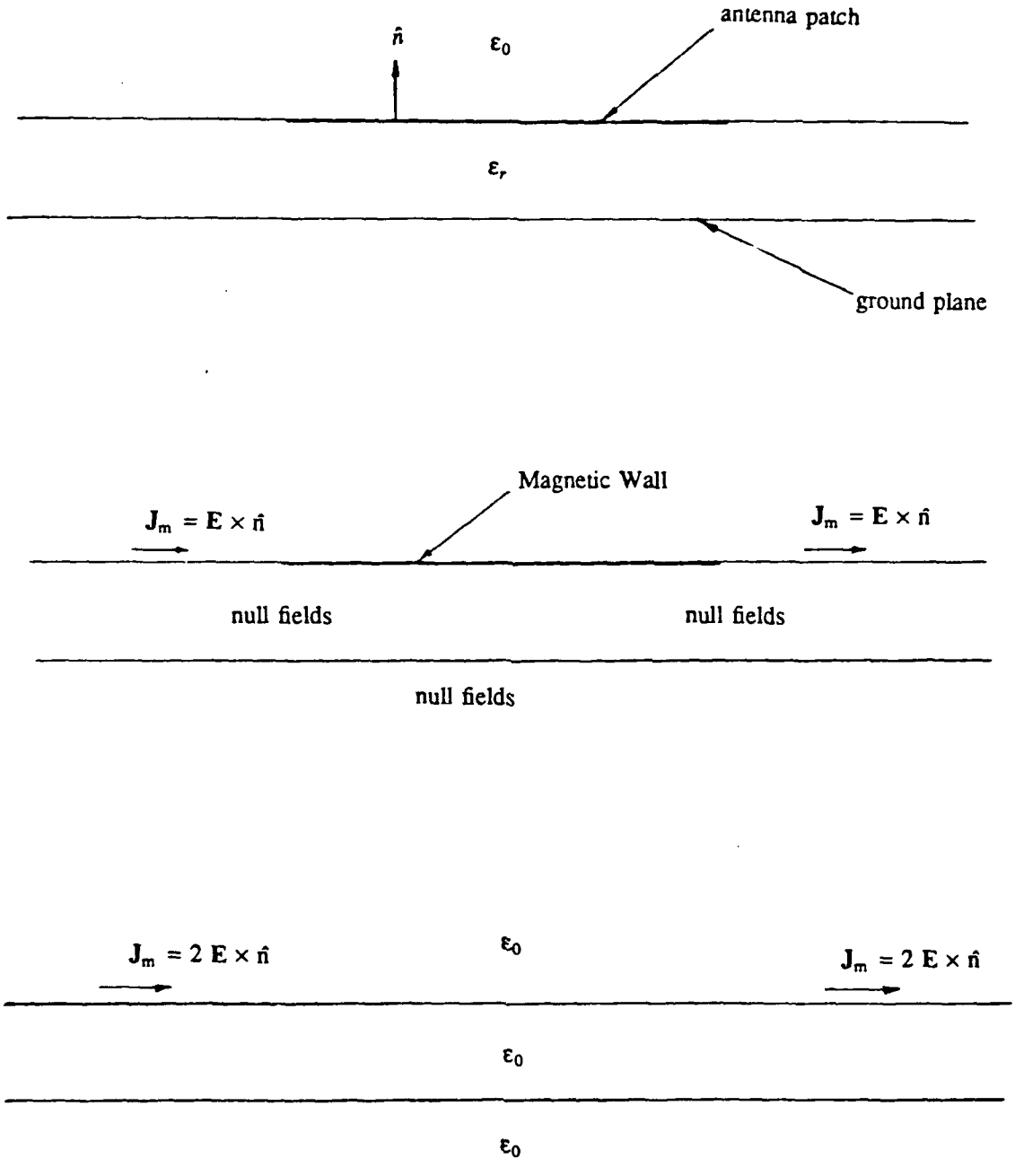

Fig. (4) The equivalent magnetic currents for computation of radiation field in the upper half space.

Top View

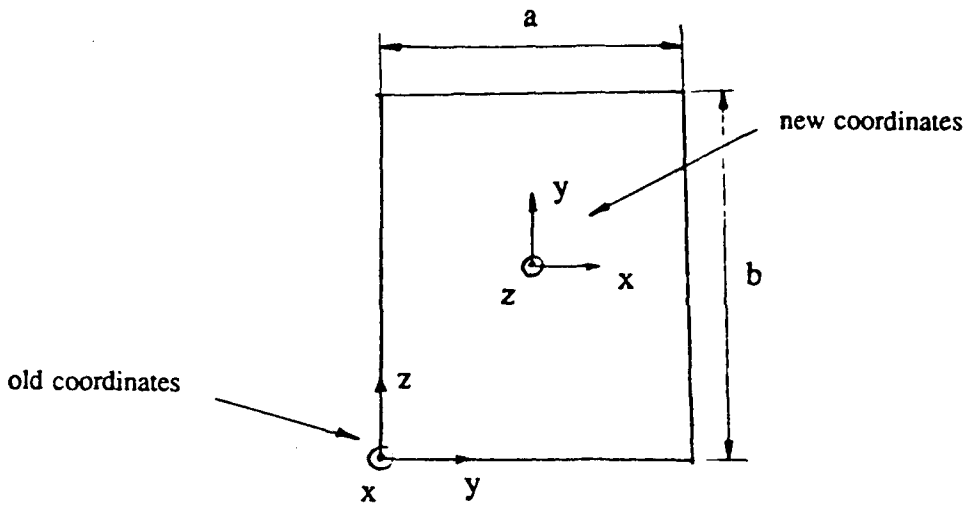

Figure (5)

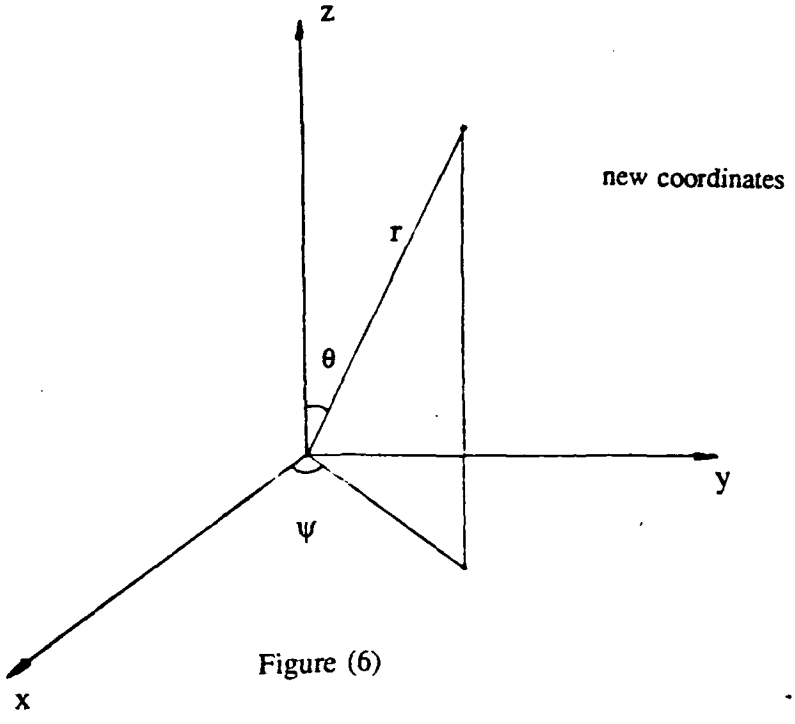

Figure (6)

Change of coordinates and coordinates for radiation pattern.

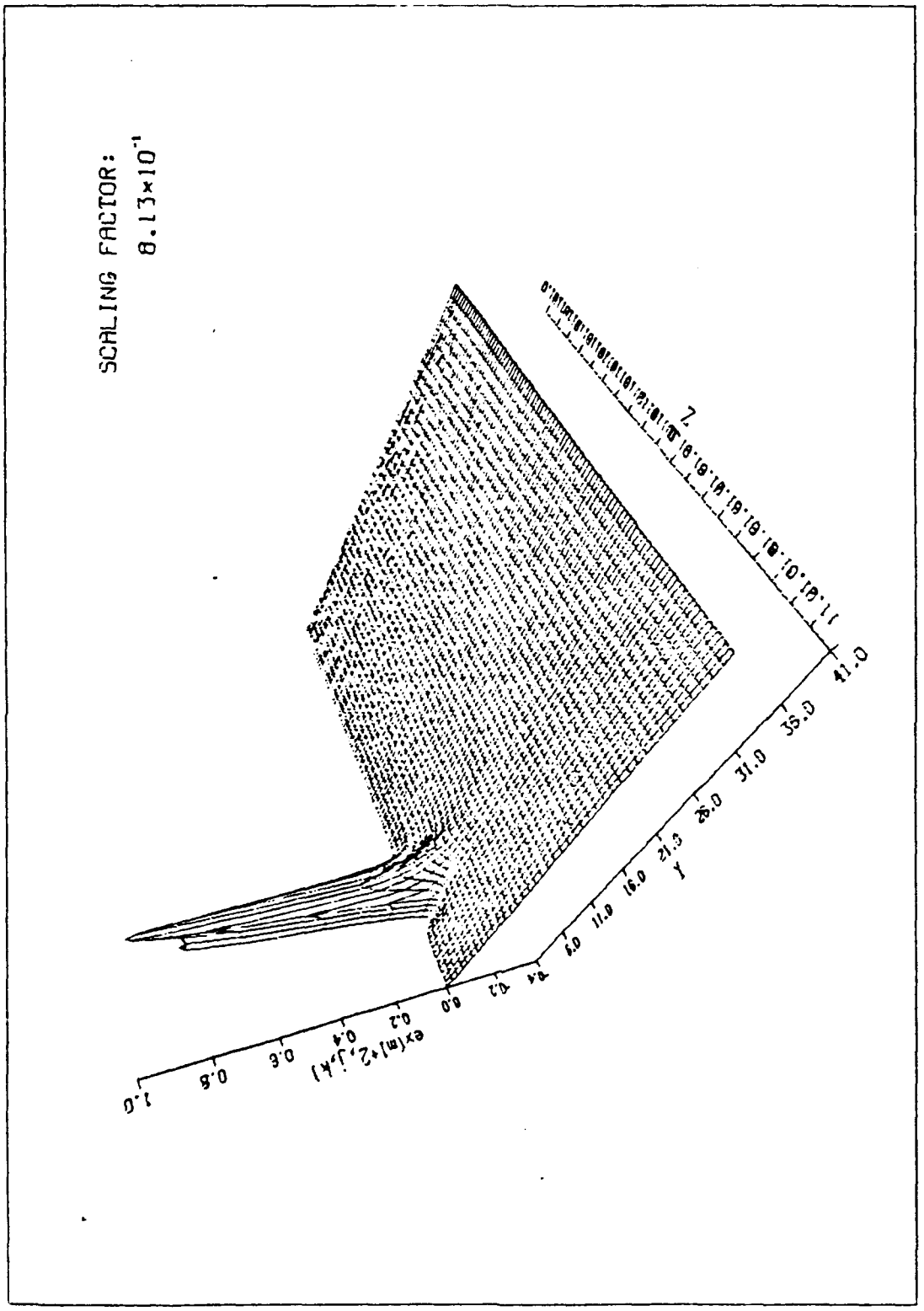

Fig. (7) Time domain E_x field distribution just underneath the microstrip line.

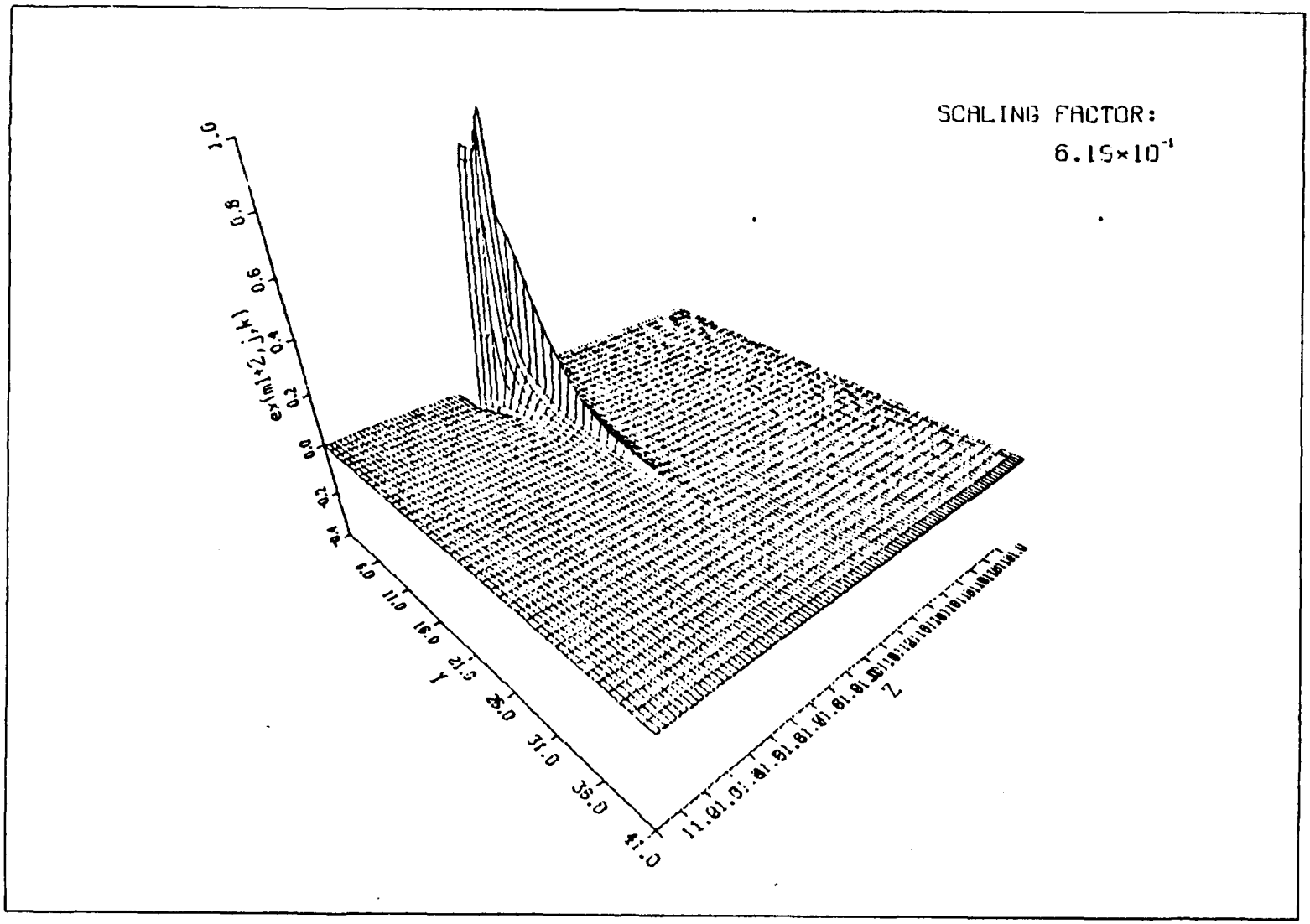

Fig. (8) Time domain E_x field distribution just underneath the microstrip line.

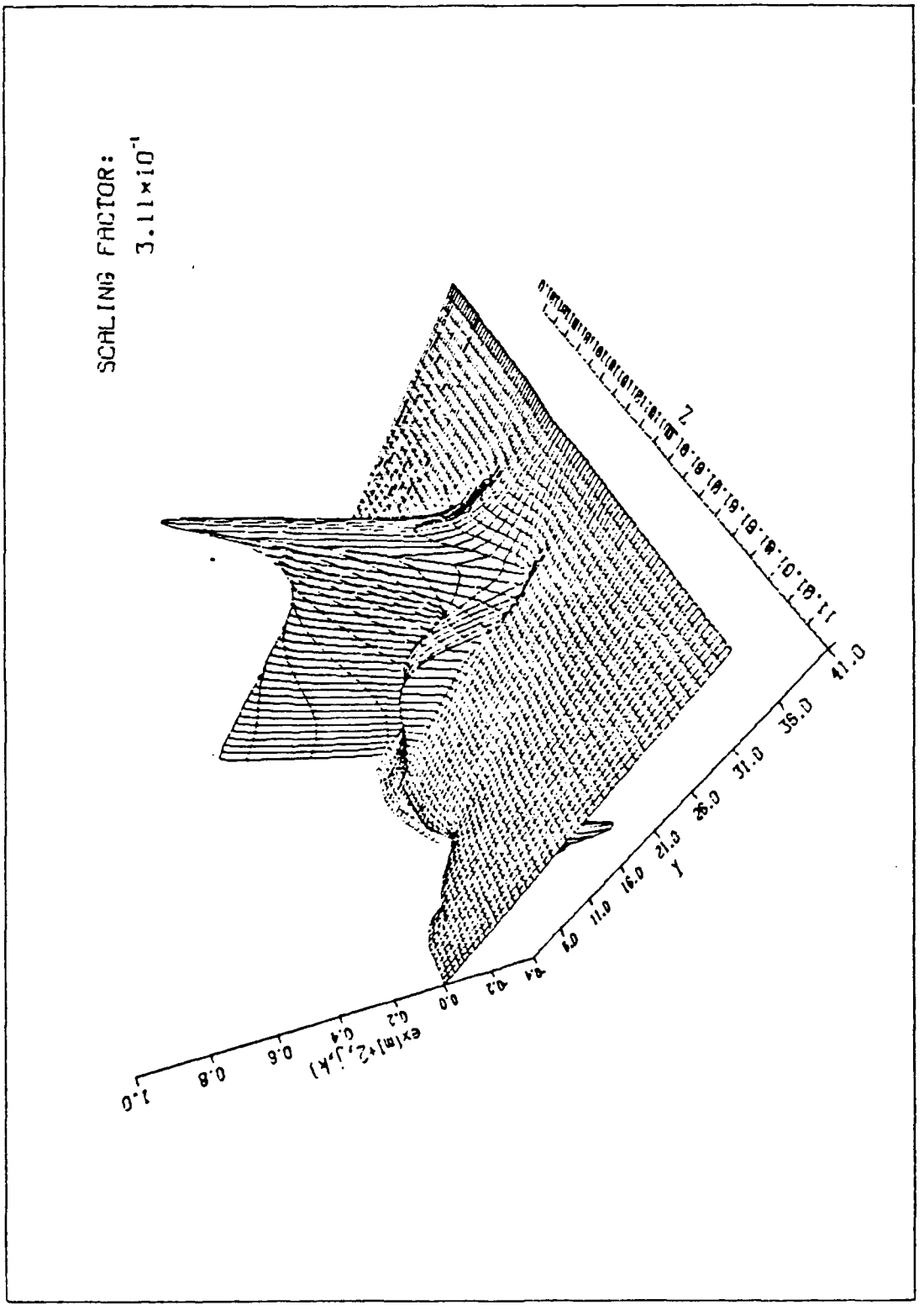

Fig. (9) Time domain E_x field distribution just underneath the microstrip line.

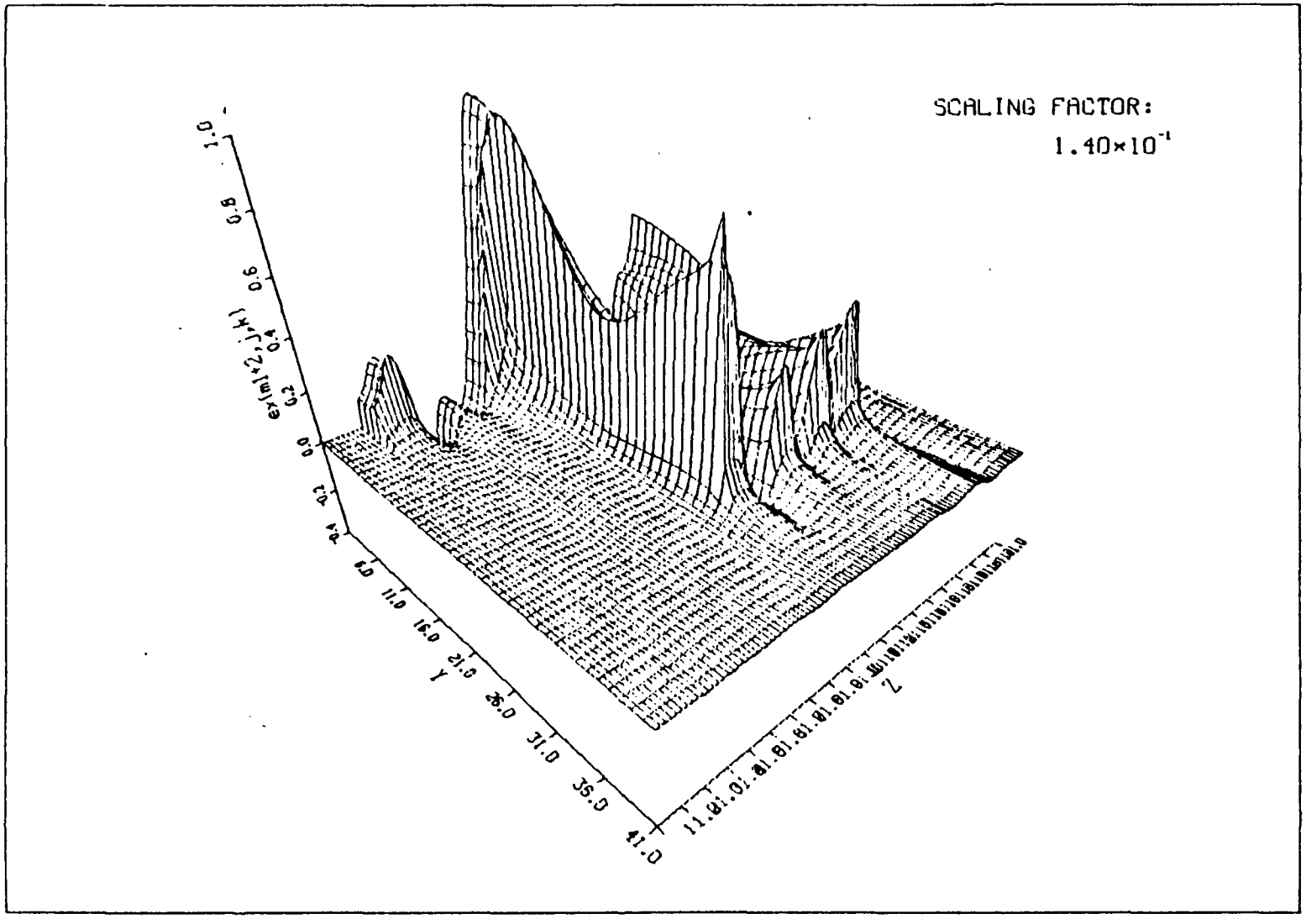

Fig. (10) Time domain E_x field distribution just underneath the microstrip line.

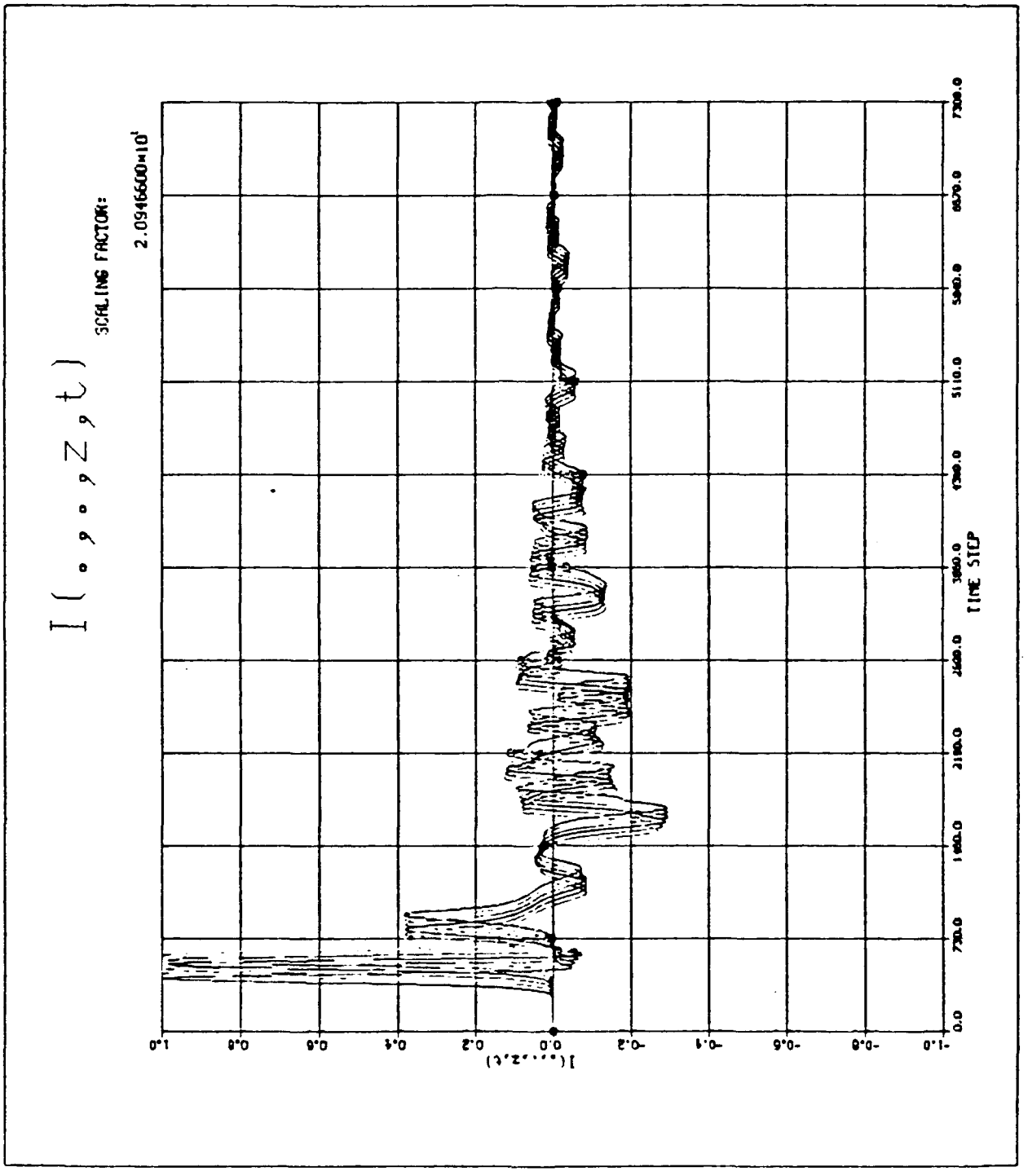

Fig. (11) The variation of time domain current, defined in (8), at fixed space point, with time.

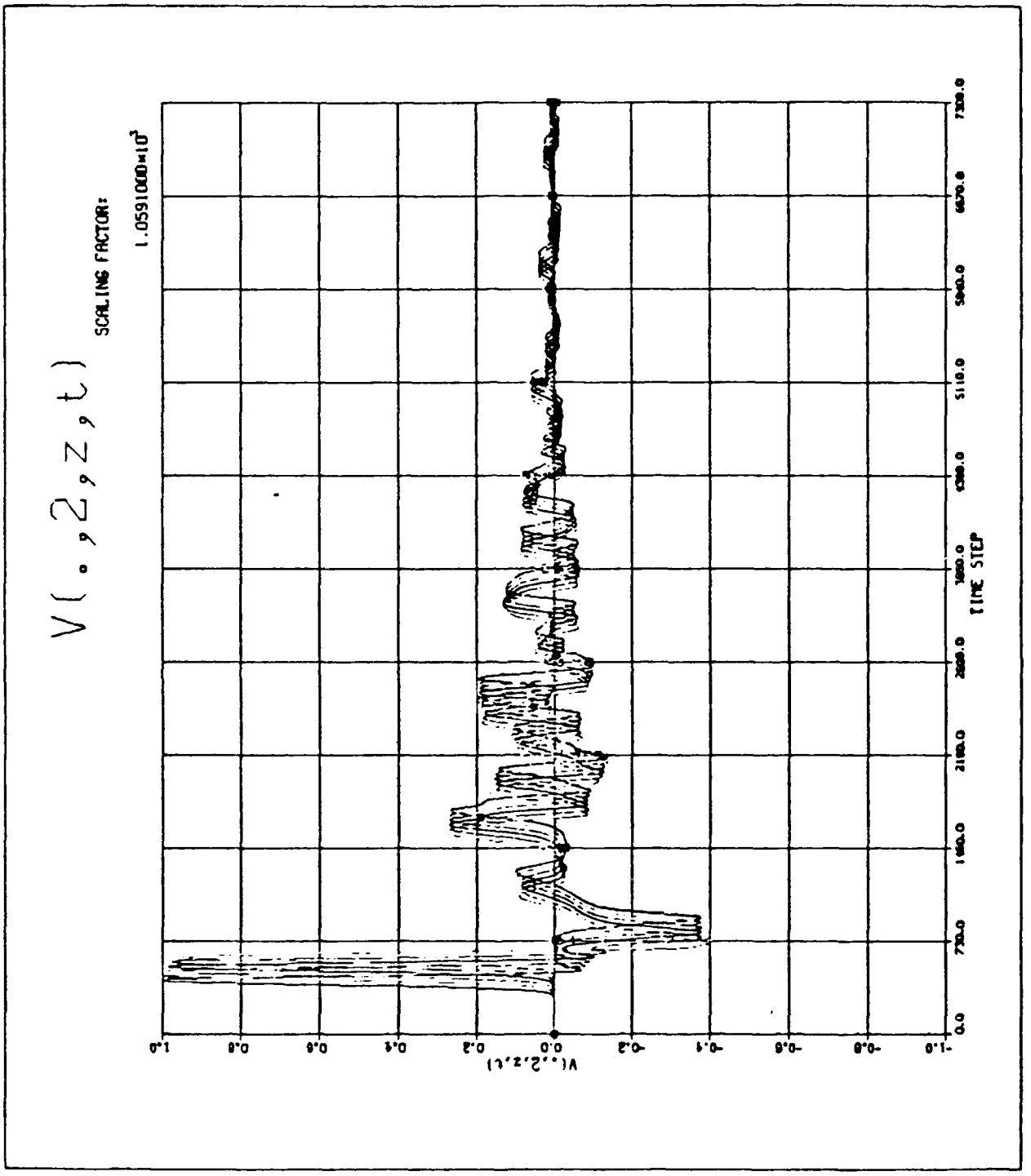

Fig. (12) The variation of time domain voltage, defined in (9), at fixed space point, with time.

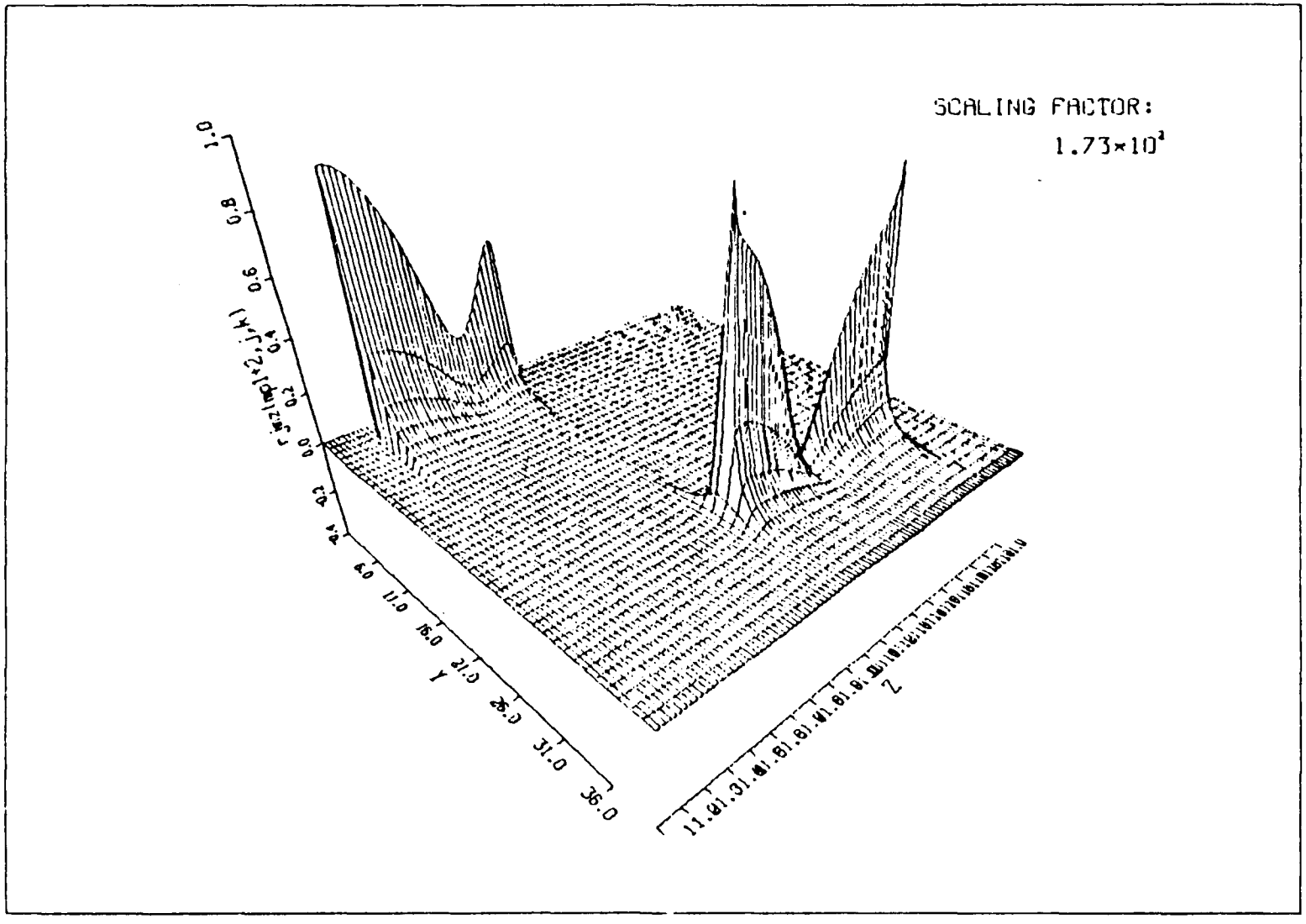

Fig. (13) Amplitude distribution of the equivalent magnetic current J_{ms} in frequency domain.

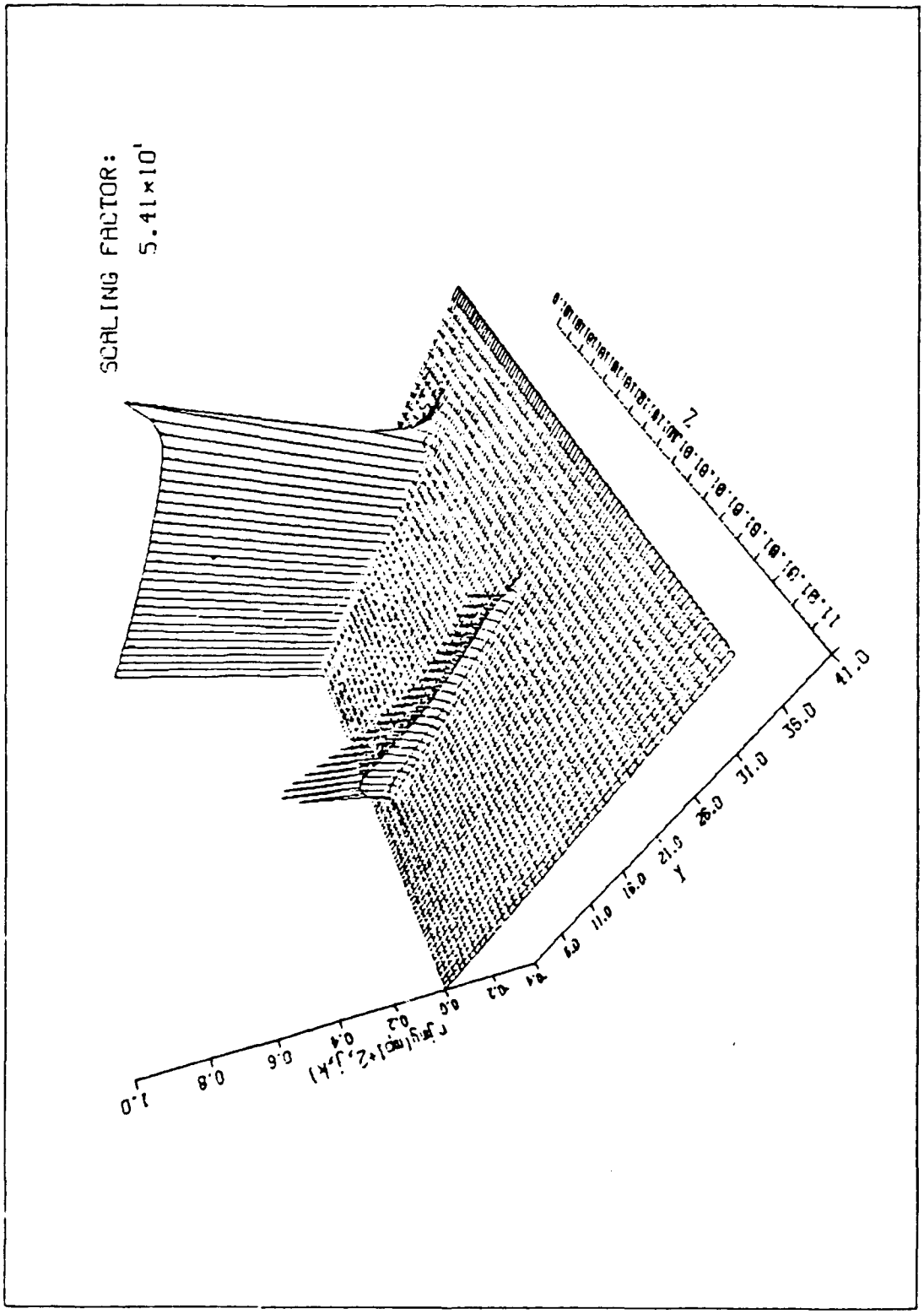

Fig. (14) Amplitude distribution of the equivalent magnetic current J_{my} in frequency domain.

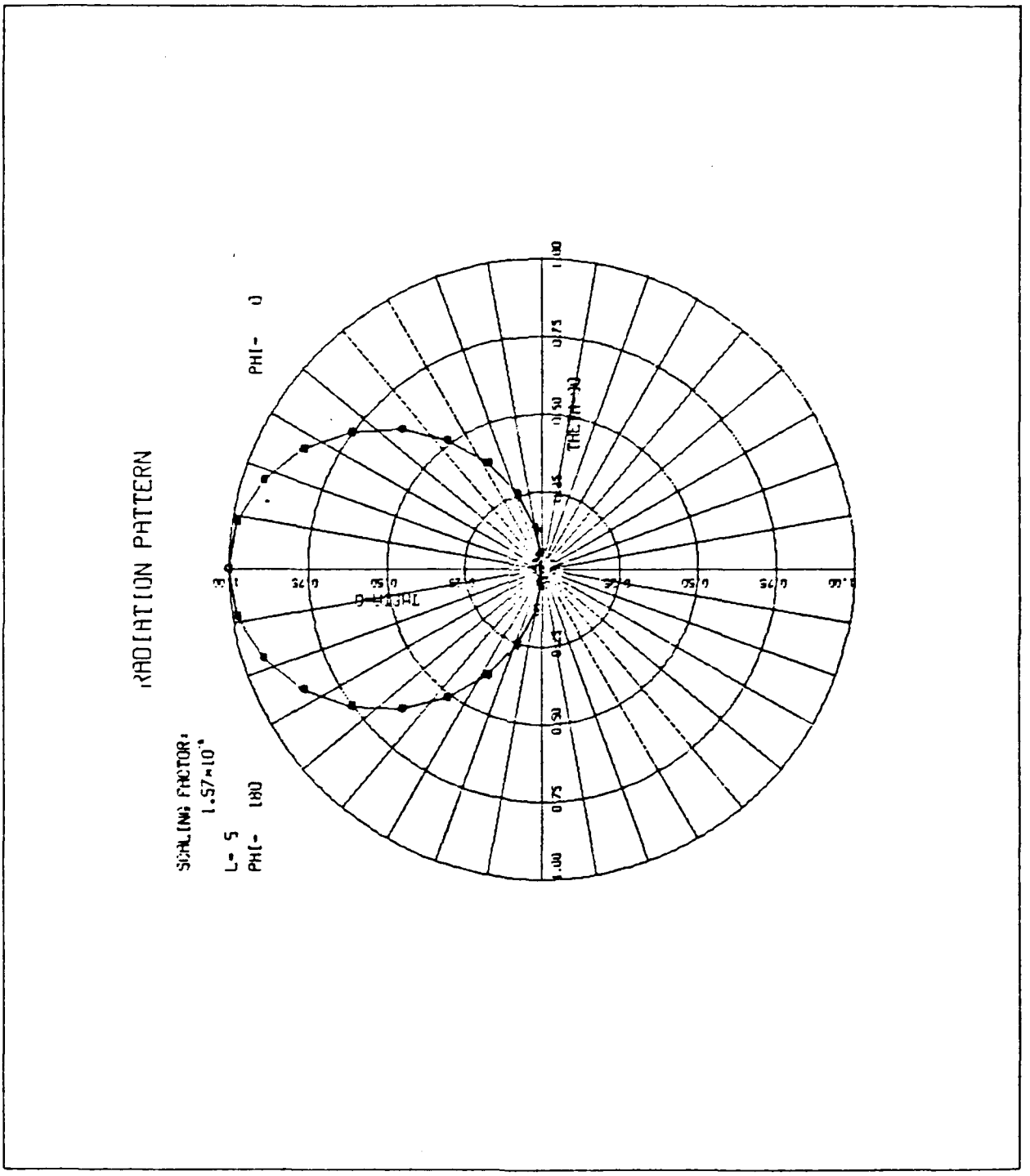

Fig. (15) Radiation pattern at resonant frequency on E-plane. The E_ϕ component is negligible here.

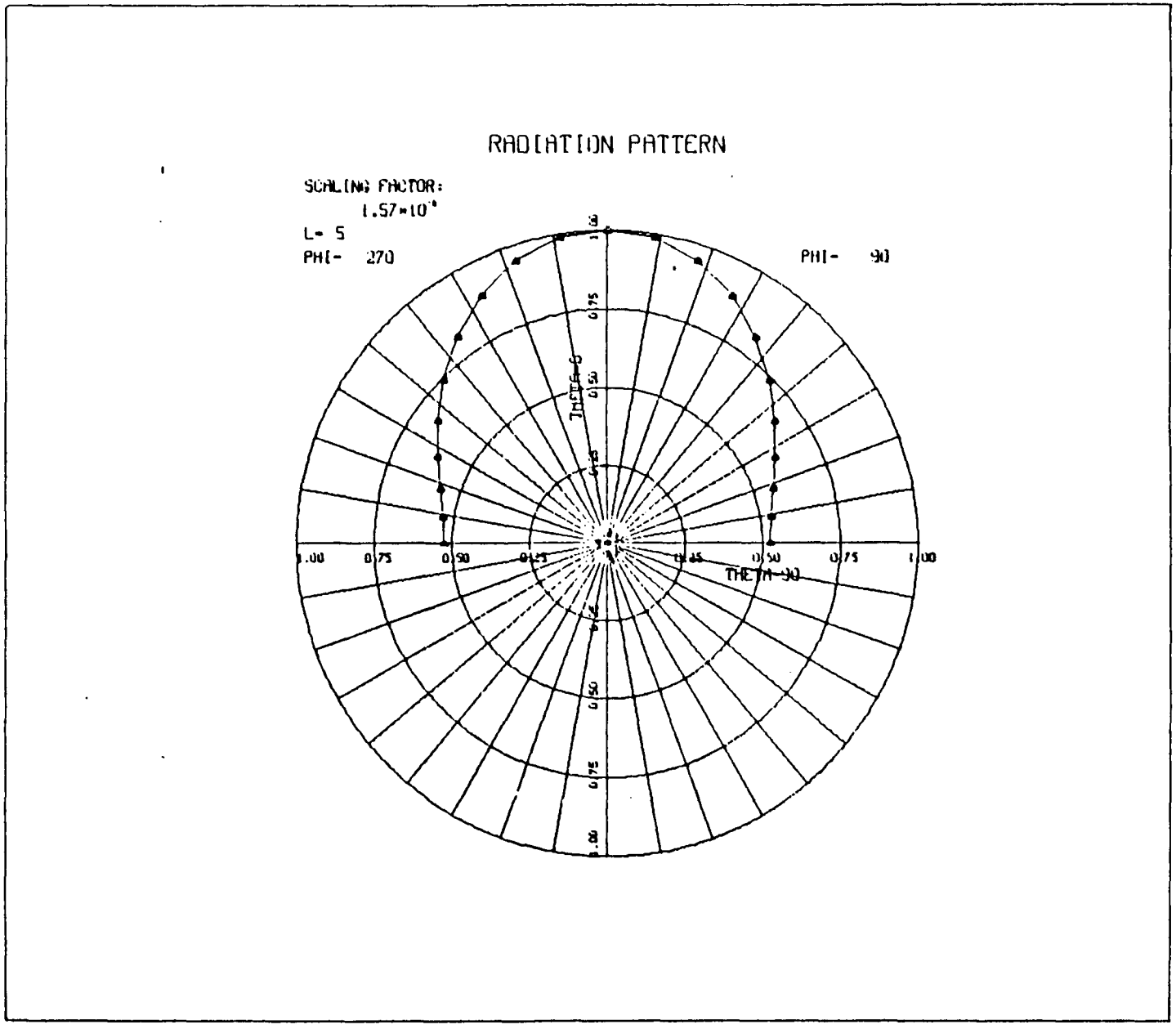

Fig. (16) Radiation pattern at resonant frequency on H-plane. The E_θ component is negligible here.

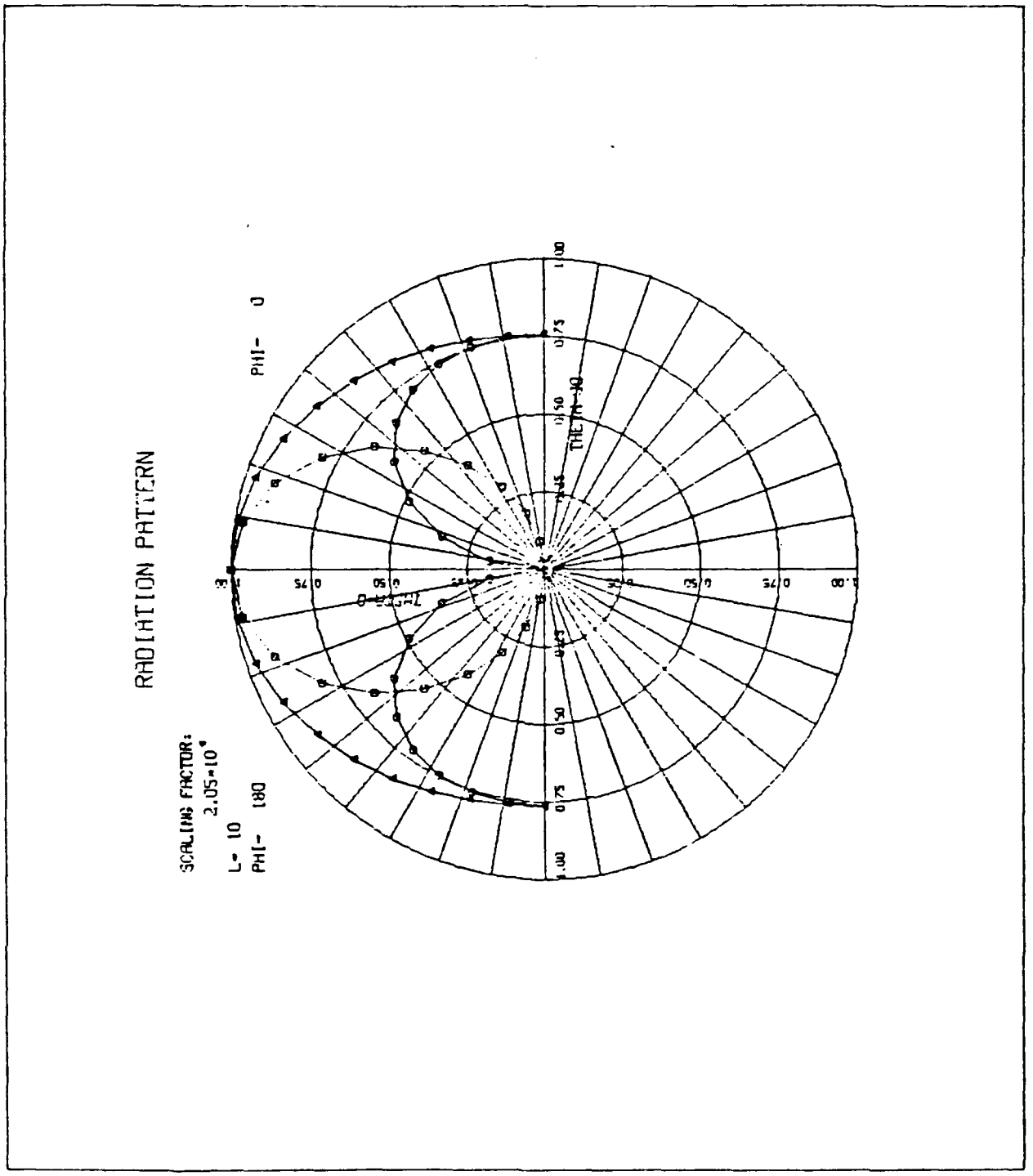

Fig. (17) Radiation pattern at resonant frequency on E-plane. The E_ϕ component is relatively small here.

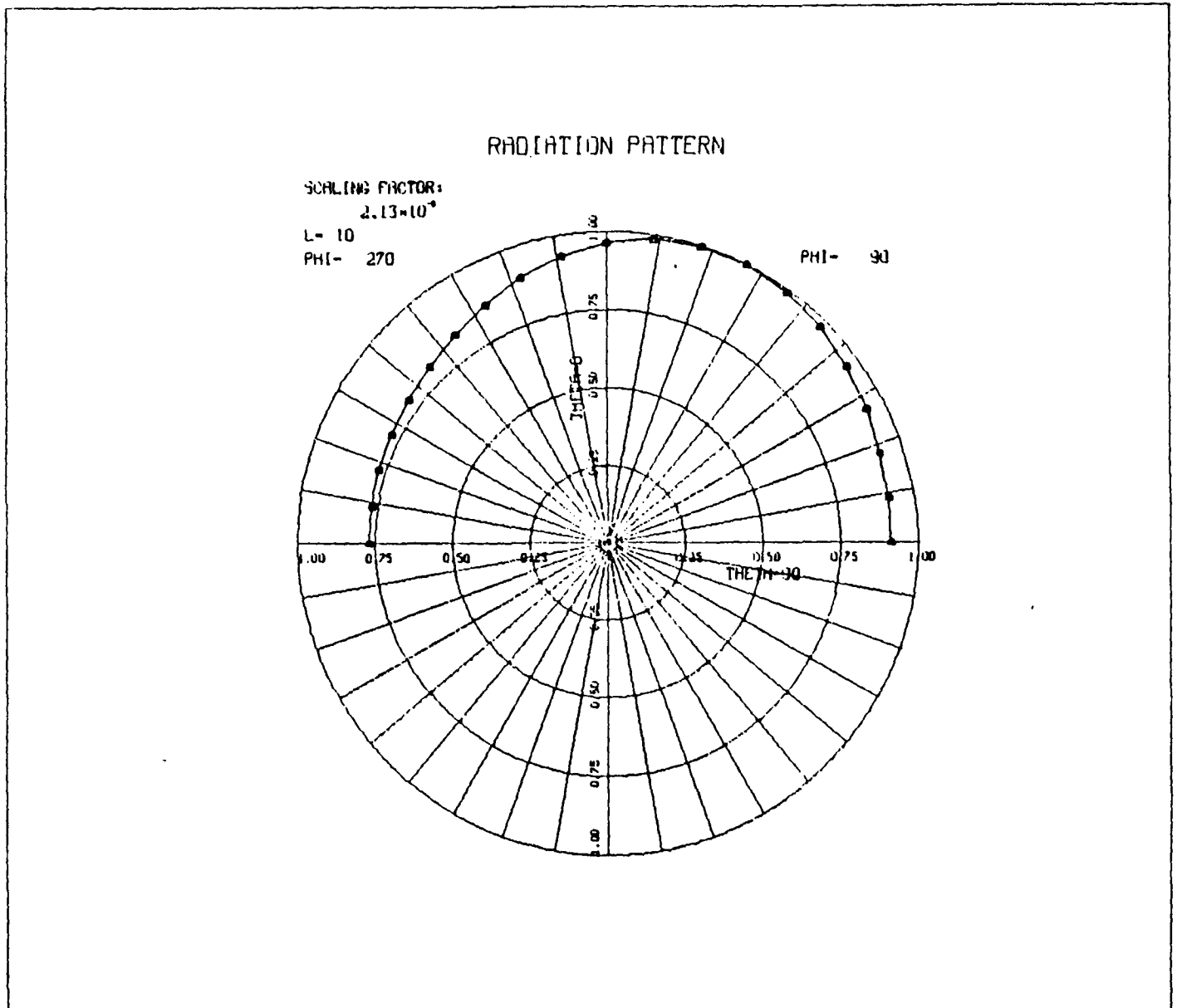

Fig. (18) Radiation pattern at resonant frequency on H-plane. The E_θ component is relatively small here.

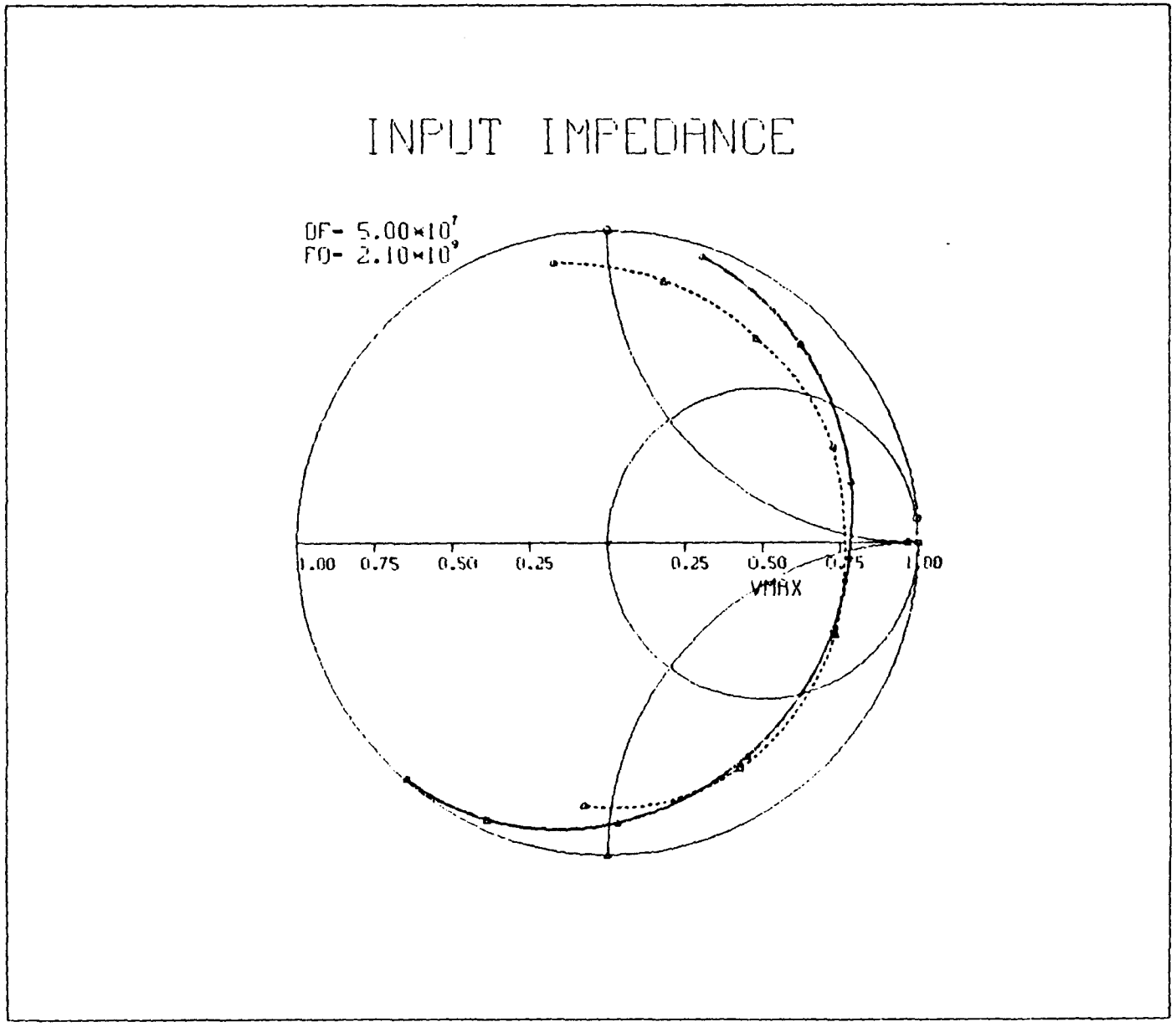

Fig. (19) Calculated input impedance loci near resonant frequency compared to measurement with $a = b = 4.02$ cm, $hp = h = 0.159$cm, $\epsilon_r = 2.55$, $w = 0.447$cm.

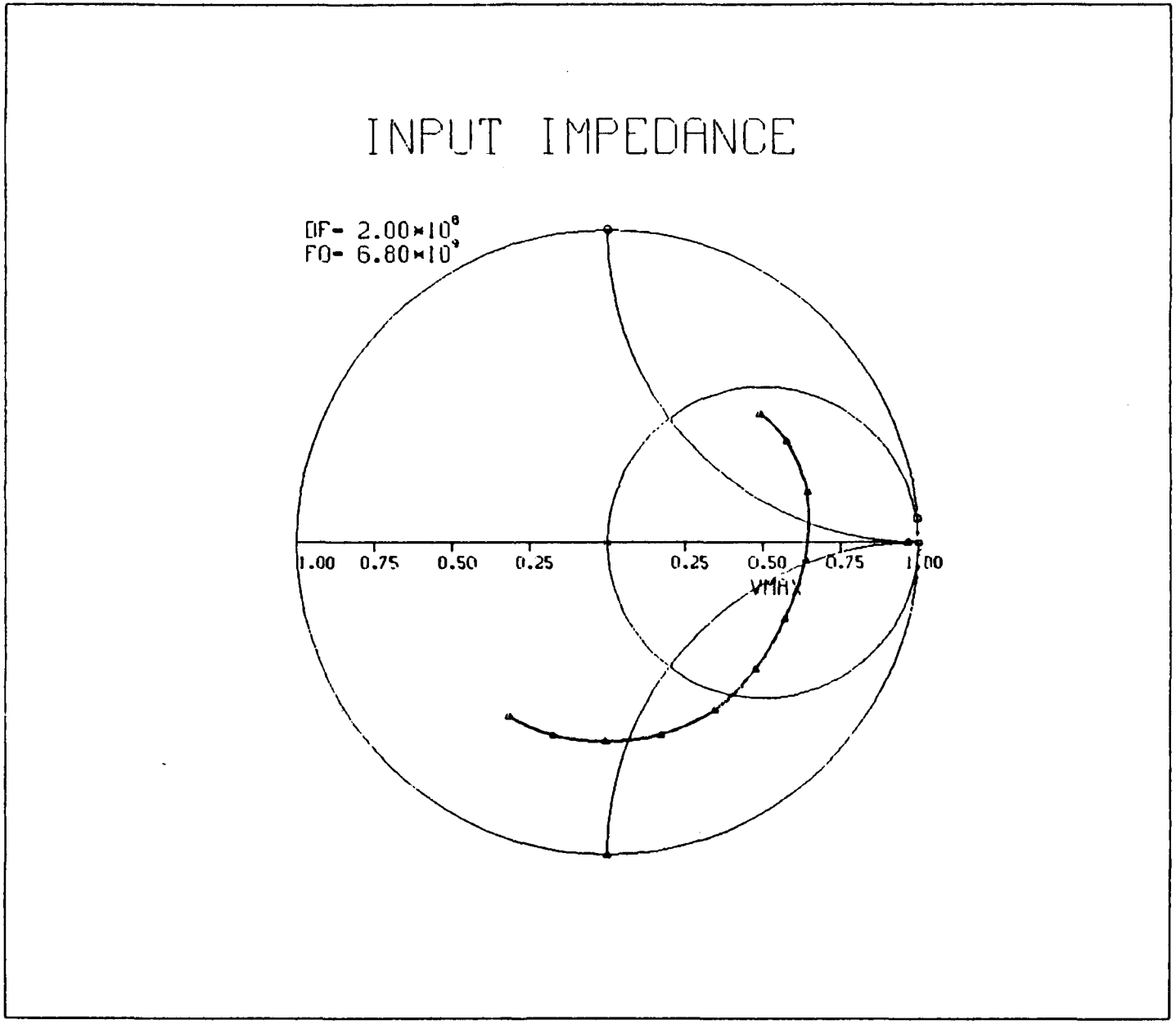

Fig. (20) Computed input impedance loci with $a = 1.7$ cm, $b = 1.1$ cm, $hp = h = 0.3175$cm, $\varepsilon_r = 2.33$.

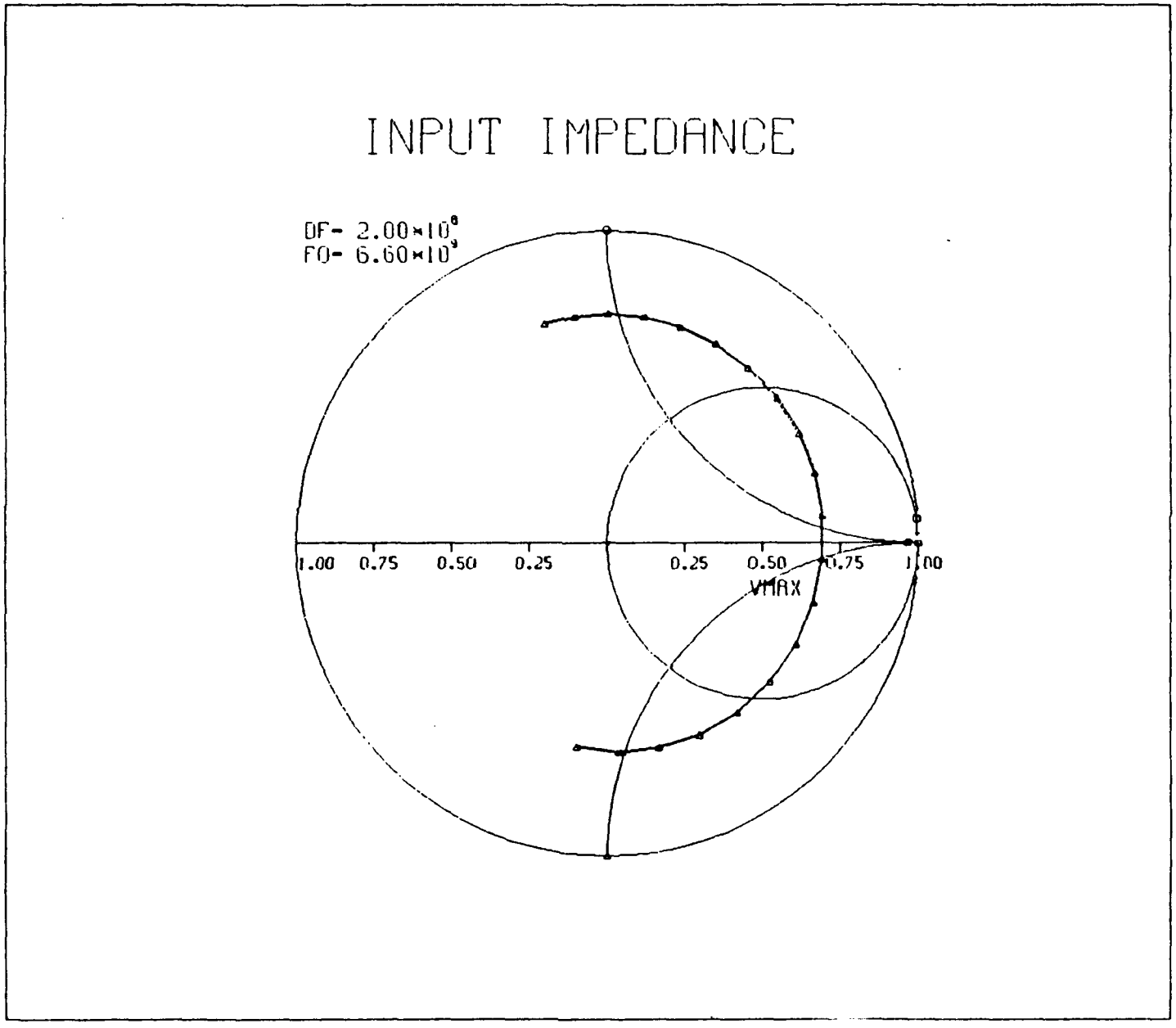

Fig. (21) Computed input impedance loci with $a = 1.4$ cm, $b = 0.9$ cm, $hp = h = 0.3175$cm, $\varepsilon_r = 2.33$.

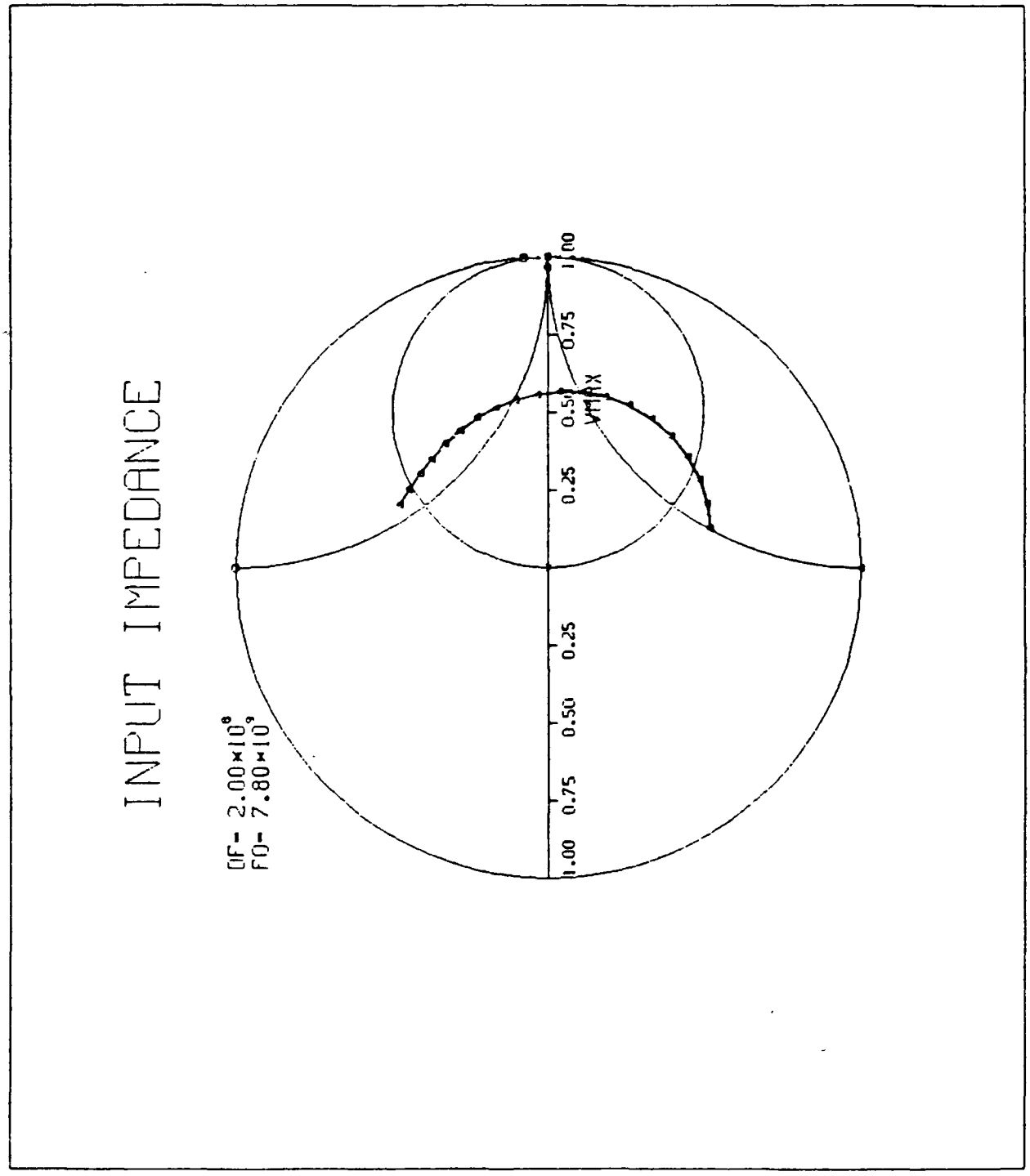

Fig. (22) Computed input impedance loci with $a = 1.2$ cm, $b = 0.8$ cm, $hp = h = 0.3175$cm, $\varepsilon_r = 2.33$.

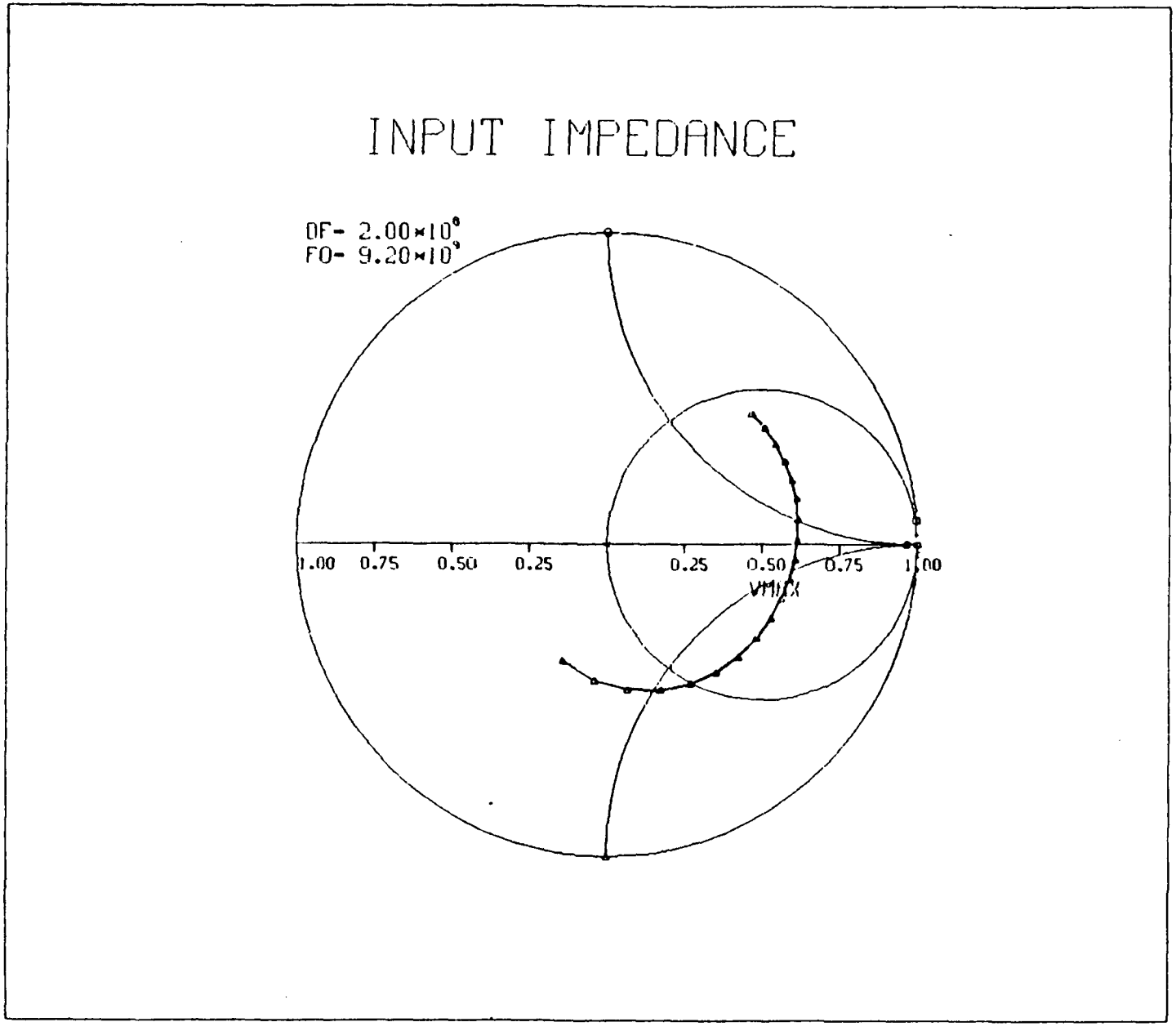

Fig. (23) Computed input impedance loci with $a = 1.05$ cm, $b = 0.7$ cm, $hp = h = 0.3175$cm, $\epsilon_r = 2.33$.

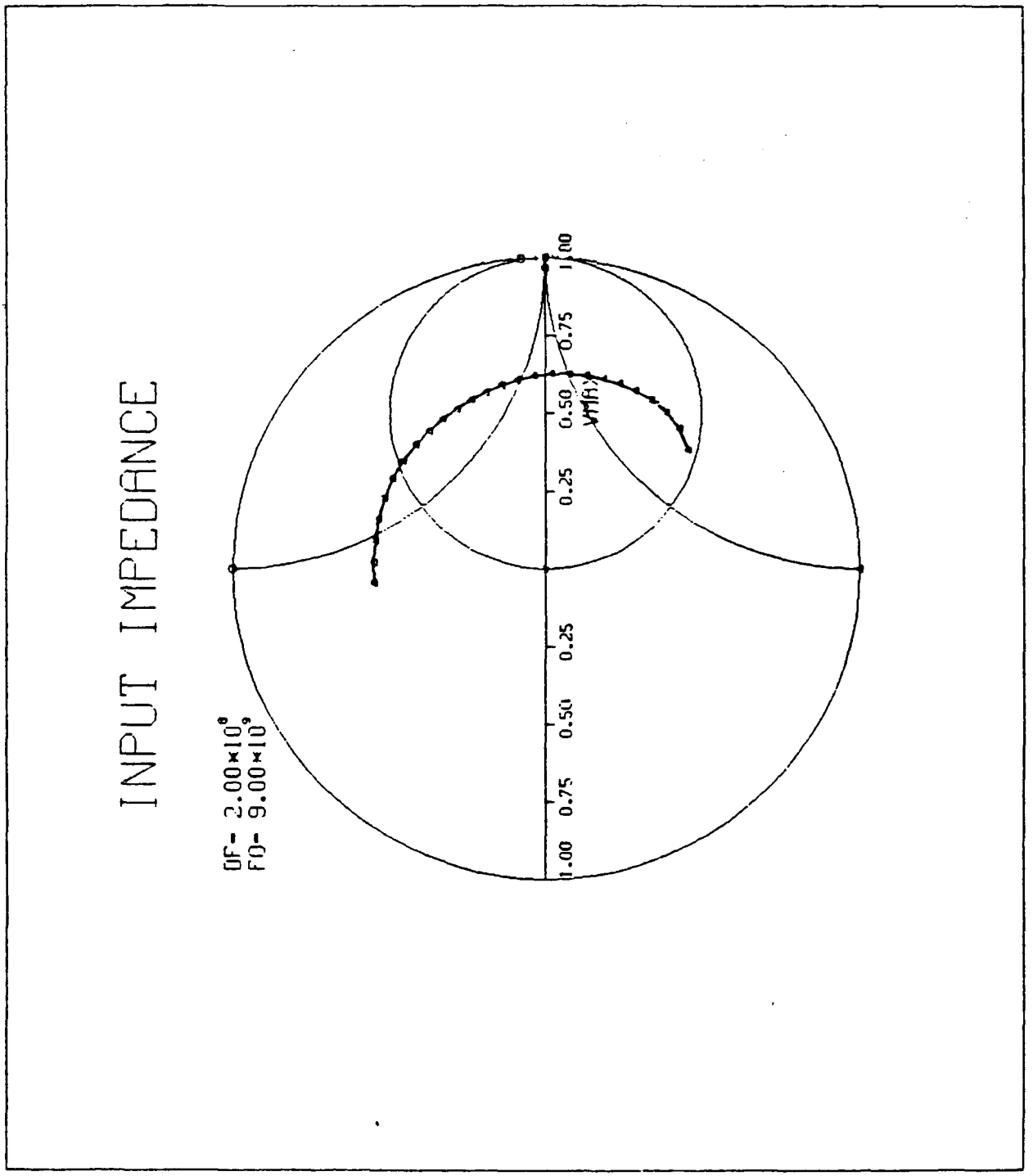

Fig. (24) Computed input impedance loci with $a = 0.9$ cm, $b = 0.6$ cm, $hp = h = 0.3175$cm, $\epsilon_r = 2.33$.